Ore Geology Reviews 88 (2017) 384–399

Contents lists available at ScienceDirect

Ore Geology Reviews

journal homepage: www.elsevier.com/locate/oregeo

Zircon U–Pb and molybdenite Re–Os geochronology, with S isotopic composition of sulfides from the Chah-Firouzeh porphyry Cu deposit, Kerman Cenozoic arc, SE Iran

Hadi Mohammaddoost [a], Majid Ghaderi [a,*], T. Vijaya Kumar [b], Jamshid Hassanzadeh [c], Saeed Alirezaei [d], Holly J. Stein [e,f], E.V.S.S.K. Babu [b]

[a] Department of Economic Geology, Tarbiat Modares University, Tehran 14115-175, Iran
[b] LAM-MC-ICP-MS National Facility, CSIR-National Geophysical Research Institute, Hyderabad, India
[c] Division of Geological and Planetary Sciences, California Institute of Technology, Pasadena, USA
[d] Faculty of Earth Sciences, Shahid Beheshti University, Tehran, Iran
[e] AIRIE Program, Colorado State University, Fort Collins, CO 80523-1482, USA
[f] CEED (Centre for Earth Evolution and Dynamics), University of Oslo, Oslo, Norway

ARTICLE INFO

Article history:
Received 11 November 2016
Received in revised form 11 May 2017
Accepted 23 May 2017
Available online 26 May 2017

Keywords:
Porphyry copper deposits
U-Pb
Re-Os
S isotopes
Chah-Firouzeh
Iran

ABSTRACT

The Chah-Firouzeh deposit with about 100 Mt ore reserves @ 0.5% Cu is a porphyry copper deposit located 14 km west of the Meiduk deposit in the northern section of the Kerman Cenozoic Magmatic Assemblage (KCMA), southeastern Iran. The mineralization is associated with a porphyry quartz-monzodiorite to quartz-diorite stock, which intruded into Eocene volcanic rocks consisting of andesite, basalt, and andesitic to dacitic tuff. Hydrothermal alteration types in the area include potassic, phyllic, and propylitic varieties. Silicic alteration locally occurred at the surface, while supergene argillic alteration overprinted the other alterations at shallow levels. Mineralization occurs as quartz-sulfide veinlets and stockworks, as well as disseminations in the porphyry body and volcanic host rocks, in association with potassic and phyllic alteration. Hypogene minerals in the deposit include pyrite, chalcopyrite, magnetite, molybdenite, and bornite. Supergene enrichment is irregularly developed in the Chah-Firouzeh deposit.

Zircon U–Pb dating of two representative samples from the Chah-Firouzeh porphyry stock yielded emplacement ages of 16.9 ± 0.4 Ma and 16.5 ± 0.2 Ma, respectively. The Early-Middle Miocene epoch marks the most important period of porphyry Cu mineralization in the KCMA. During this period, many adakitic magmas intruded the Eocene volcano-sedimentary sequences and formed some of the largest porphyry copper deposits in Iran, such as Sarcheshmeh and Meiduk. Molybdenite Re–Os dating on two samples separated from "B and D type" veinlets show that mineralization occurred at 16.60 ± 0.06 Ma and 15.99 ± 0.06 Ma, implying a time span of about 0.6 Ma for mineralization.

The $\delta^{34}S$ values for molybdenite, chalcopyrite, and pyrite from "A, B, and D type" veinlets vary from −1.4 to +2.5‰ suggesting a magmatic source for sulfur. The calculated temperatures for sulfide pairs are compatible with those obtained from fluid inclusion microthermometry and show isotope equilibrium due to fluid evolution.

1. Introduction

The Urumieh-Dokhtar Magmatic Arc (UDMA), west central Iran, is a significant host to porphyry copper deposits (PCDs) (e.g., Shahabpour and Kramers, 1987; Hassanzadeh, 1993; McInnes et al., 2005; Shafiei et al., 2009; Alirezaei and Hassanpour, 2011; Richards et al., 2012). Most known porphyry systems, including the world-class Sarcheshmeh together with Meiduk, Daraloo and other major deposits occur in the southern segment of the UDMA, known as Kerman Cenozoic Magmatic Assemblage (KCMA) (Fig. 1) (Dimitrijevic, 1973; Shafiei, 2008). The KCMA, ~500 km long and 40–80 km wide, is dominated by Eocene normal calc-alkaline mafic to felsic lava flows and pyroclastic materials, Oligocene granitoid bodies, some of batholith sizes, and shallow Miocene

* Corresponding author.
E-mail address: mghaderi@modares.ac.ir (M. Ghaderi).

http://dx.doi.org/10.1016/j.oregeorev.2017.05.023
0169-1368/

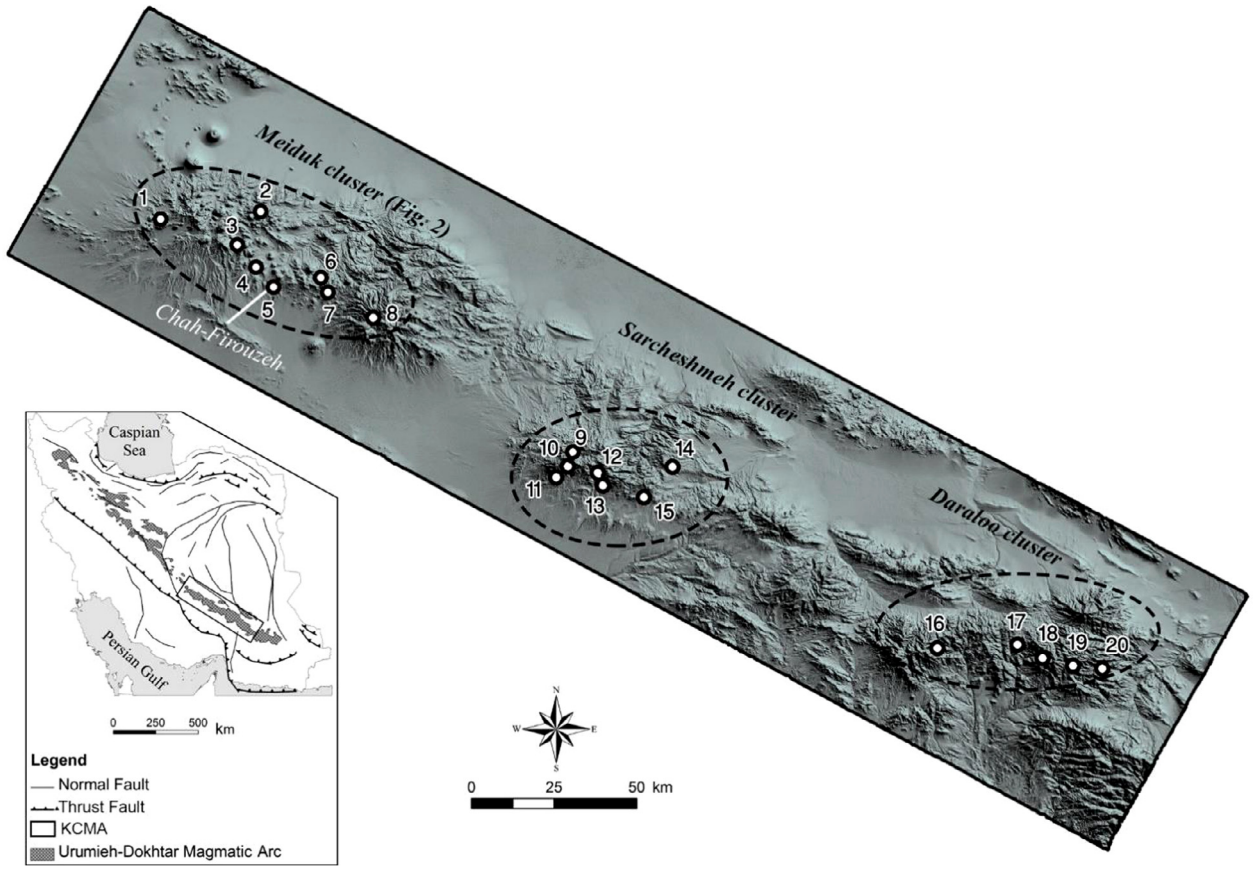

Fig. 1. Distribution of porphyry copper deposits in three major clusters (Meiduk, Sarcheshmeh and Daraloo) in the KCMA. The Chah-Firouzeh deposit lies in the Meiduk cluster is shown here. 1. Kader, 2. Gode-Kolvari, 3. Iju, 4. Serenu, 5. Chah-Firouzeh, 6. Parkam, 7. Meiduk, 8. Abdar, 9. Sarcheshmeh, 10. Nochoon, 11. Sarkuh, 12. Salpak, 13. Darreh Zar, 14. Kuh Panj, 15. Bagh Khoshk, 16. Daraloo, 17. Sarmeshk, 18. Bondar Hanza, 19. Gorouh, 20. Bab Torosh. Shaded relief map from SRTM Global Digital Elevation Model, U.S. Geological Survey, EROS Data Center.

adakite-like intrusions (e.g., Dimitrijevic, 1973; Hassanzadeh, 1993; Atapour and Aftabi, 2007; Taghipour et al., 2008).

Generally accepted mechanisms for this magmatic arc are related to successive stages of the Neotethyan ocean closure and subduction beneath Central Iran during Paleogene and subsequent continent-continent collision in Neogene (e.g., Förster, 1978; Berberian and King, 1981; Berberian et al., 1982; Dercourt et al., 1986; Mohajjel et al., 2003; Allen et al., 2004; Agard et al., 2005; Shafiei, 2008).

The Chah-Firouzeh PCD (over 100 Mt @ 0.5% Cu) (NICICo, 2009) is located in the northwestern part of the KCMA,~14 km west of the Meiduk copper mine (Fig. 1). Mineralization is associated with a porphyry quartz-monzodiorite to quartz-diorite stock intruded into Eocene andesitic to basaltic volcanic rocks (Mohammadzadeh, 2009; Einali et al., 2014).

Hydrothermal alteration assemblages typical of porphyry copper systems are reported from Chah-Firouzeh, with a central potassic core that grades outward to phyllic and propylitic assemblages (Mohammadzadeh, 2009). Copper mineralization in the Chah-Firouzeh occurs as stockwork, scattered vein-veinlets and dissemination in the porphyry body and weakly in andesitic and in the volcanic host rocks.

Formation of the PCDs is linked in time and space with specific events in the evolution of the associated magmatic belts (e.g., Richards, 2009; Shafiei et al., 2009; Sillitoe, 2010). Due to the great potential for PCDs in the KCMA and possibly in other magmatic assemblages in Iran, it is important to gain insight into the timing of various events leading to the formation of porphyry deposits located in this area.

In this paper, we report zircon U–Pb and molybdenite Re–Os ages constraining the timing of emplacement/crystallization of the porphyry stock and associated mineralization in the Chah-Firouzeh PCD. Due to the importance of studying sulfur isotopes in determining the origin of mineralizing fluids, sulfur isotope compositions will also be discussed.

2. Geological background

Magmatism in the KCMA is mainly related to Eocene to Miocene volcano-plutonic activities, with the peak of volcanism in middle Eocene and plutonism in Oligo-Miocene (Dimitrijevic, 1973; Hassanzadeh, 1993) and the PCDs dominantly occurred during this period.

During the early Eocene, arc magmatism started in the KCMA in a marine environment. This activity dominantly includes basic to felsic effusive volcanic and pyroclastic rocks in association with sedimentary interlayers (Bahr-Aseman complex) (Dimitrijevic, 1973; Hassanzadeh, 1993). The next magmatic activity occurred during middle-late Eocene and formed basaltic to rhyolitic volcaniclastic sequences in association with sedimentary marine interlayers (Razak complex) and granitoid intrusives (Jebal-Barez type). These volcanic and intrusive suites show a calc-alkaline to locally tholeiitic affinity (Ahmad and Posht Kuhi, 1993). During the late Eocene to middle Oligocene, magmatic activity followed to a more limited extent and generated volcanic (Hezar complex) and associated plutonic rocks with a high-K calc-alkaline and shoshonitic nature (Hassanzadeh, 1993). Middle-late Miocene magmatism in

the KCMA is characterized by emplacement of shallow level plutons (Kuh Panj type) (McInnes et al., 2005) and continued to the Pliocene represented by sub-volcanic bodies, stratovolcanoes, and numerous dacitic to rhyolitic domes (Dimitrijevic, 1973; Shafiei, 2008).

Porphyry copper mineralization in the KCMA is associated with younger porphyritic Kuh Panj type granitoids, and the earlier Jebal-Barez type granitoids are barren (e.g., McInnes et al., 2003; Shafiei et al., 2009) or weakly mineralized. Porphyry copper deposits in the KCMA are distributed in three major clusters including from northwest to southeast, Meiduk cluster, Sarcheshmeh cluster and Daraloo cluster (Alimohammadi et al., 2015).

The Chah-Firouzeh, Meiduk, Parkam, Abdar, Iju, Serenu, Gode-Kolvari, and some smaller prospects, occur in the "Meiduk cluster" in the northwestern part of the KCMA (Fig. 2). The country rocks include Eocene volcanic and volcanic-sedimentary rocks, dominantly flysch, conglomerate, sandstone, limestone, and marl together with volcanogenic sequences. These units are strongly folded and faulted and intruded by granitic plutons.

The Chah-Firouzeh deposit is surrounded by volcano-sedimentary rocks mainly andesite to dacite, tuff, volcaniclastic conglomerate, lahar and Quaternary deposits. Mineralization in the Chah-Firouzeh is associated with a quartz diorite to quartz monzodiorite porphyry stock (Fig. 3) known as "Chah-Firouzeh porphyry" (Einali et al., 2014) intruded into andesitic to basaltic host rocks (Fig. 4a) and (Fig. 5). The intrusive body is characterized by phenocrysts of quartz, plagioclase, biotite, and minor hornblende in a microgranular quartz-feldspar groundmass (Fig. 6 and Fig. 7).

Mineralogical composition of the Chah-Firouzeh porphyry consists, in the least altered rocks, of 40–50% plagioclase, 10–15% quartz, and about 10% biotite and hornblende phenocrysts, distributed in a medium- to fine-grained groundmass of about 25% quartz, plagioclase, and K-feldspar. Accessory minerals include magnetite, apatite, and zircon. Magmatic biotite phenocrysts occur as euhedral to subhedral crystals 1 to 5 mm in diameter. Plagioclase, dominantly of andesine-oligoclase composition (Einali et al., 2014) occurs as euhedral to subhedral phenocrysts 1–5 mm long, and locally displays compositional zoning (Fig. 7 a and b). A distinct feature in outcrops in the southern part of the deposit, where high-grade copper oxide ores were mined in the past, is the partial replacement of plagioclase phenocrysts by malachite. Hornblende, where present, occurs as euhedral elongated crystals, 2–6 mm long. Quartz is a common constituent both as

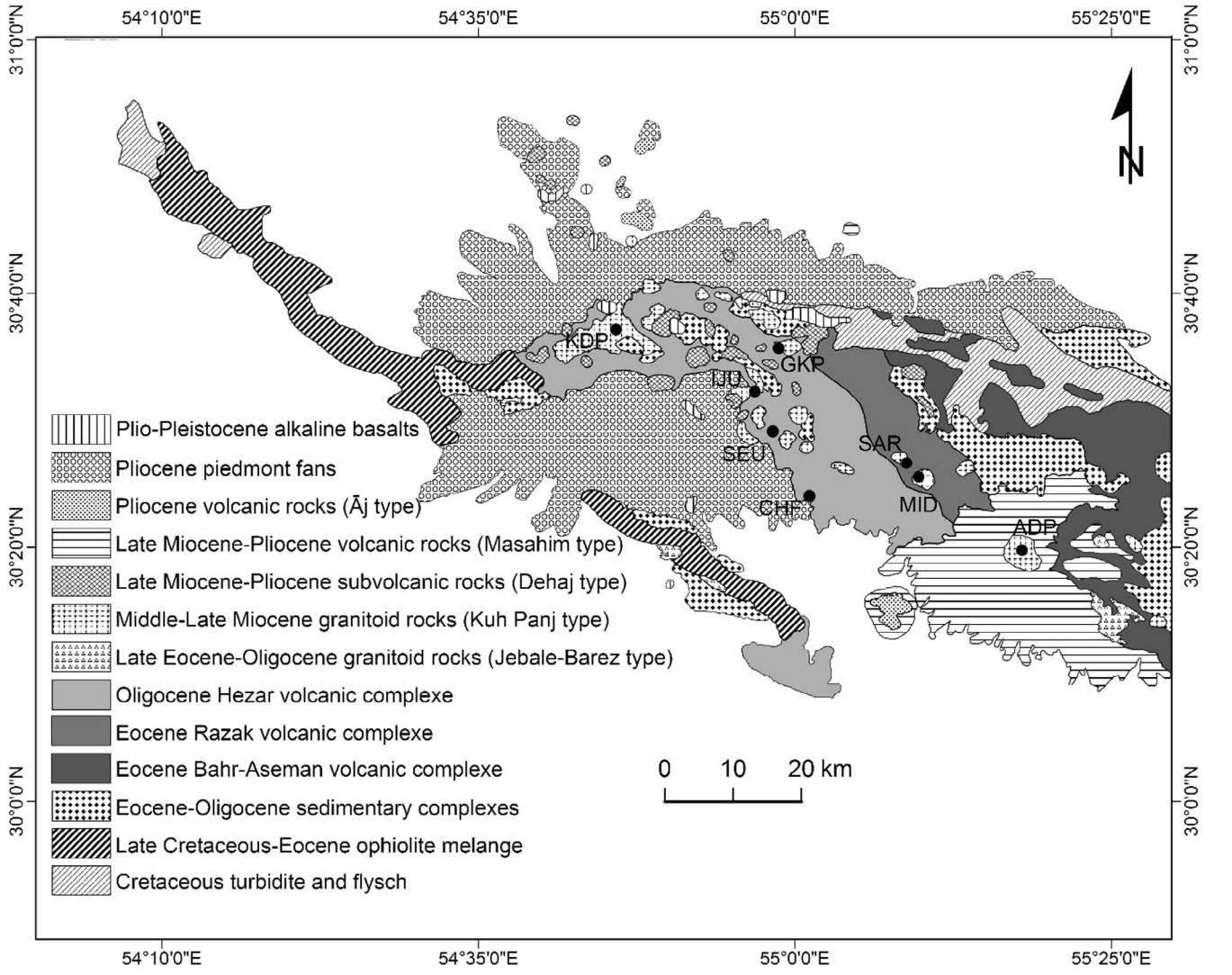

Fig. 2. Geological map of northwest part of KCMA (Meiduk cluster) and distribution of porphyry copper deposits/prospects. (simplified from Anar 1:250,000 geological map (Geological Survey of Iran) and (Honarmand et al., 2011). Abbreviations: ADP Abdar prospect, CHF Chah-Firouzeh deposit, GKP Gode-Kolvari prospect, IJU Iju deposit, KDP Kader prospect, MID Meiduk deposit, SAR Sara (Parkam) prospect.

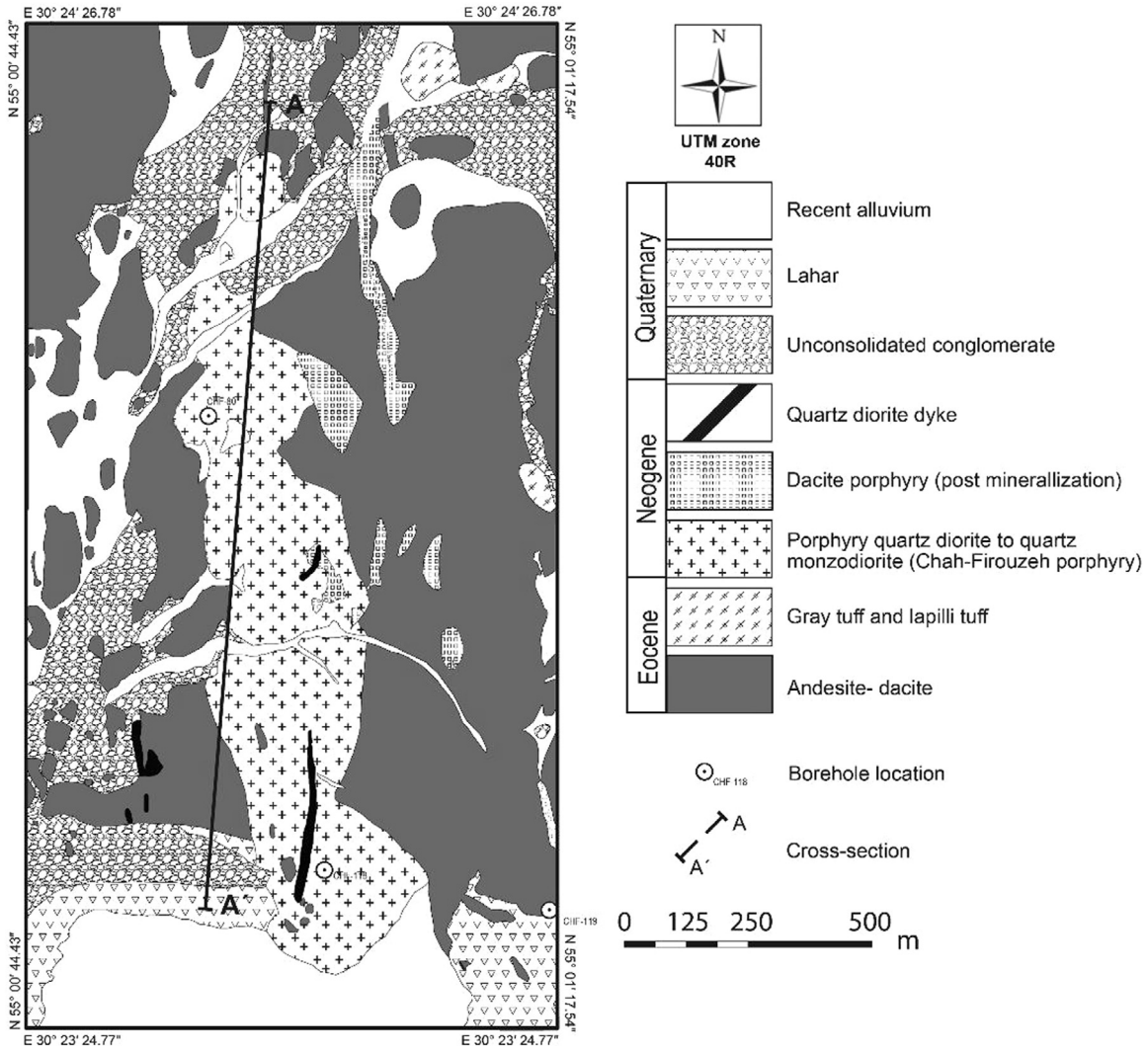

Fig. 3. Geological map of the Chah-Firouzeh porphyry Cu deposit. Simplified and modified after NICICo Internal report (2009).

euhedral to rounded and resorbed phenocrysts, and as fine crystals in the groundmass.

Eocene andesitic to dacitic host rocks show porphyritic to microgranular texture and mineral composition in these units distinguished by quartz, plagioclase, hornblende, biotite and augite phenocrysts distributed in a fine-grained groundmass of quartz, plagioclase, K-feldspar, and opaque minerals (Fig. 7 c, d).

The Chah-Firouzeh porphyry and the volcanic host rocks are cut by a set of post-ore diorite to quartz diorite dykes (Einali et al., 2014) that mainly outcropped in southern part of the area (Fig. 3). These units are distinguished by quartz, plagioclase, hornblende, and biotite phenocrysts in a microgranular quartz-feldspar context (Fig. 7 e) Late and post-mineralization dykes with different composition are the most common characteristic of PCDs in the KCMA (Shafiei et al., 2009; Aghazadeh et al., 2015).

A set of fresh dacitic domes and subvolcanic bodies are the youngest igneous units in the Chah-Firouzeh that are exposed mainly in the northeastern part of the deposit. The dacitic unit contains many enclaves of the altered and mineralized Chah-Firouzeh porphyry body. The dacitic rocks are characterized by quartz, plagioclase, hornblende, and biotite phenocrysts in a fine feldspar-quartz groundmass (Fig. 7f).

Alteration assemblages typical of porphyry copper systems are well-developed in the Chah-Firouzeh (Alirezaei and Mohammadzadeh, 2009). Potassic alteration is characterized by biotite ± K-feldspar + magnetite ± anhydrite. The alteration affected both the Chah-Firouzeh porphyry intrusion and the andesitic to basaltic host rocks. Phyllic alteration is widespread and occurs as irregular patches within, as well as a distinct shell around, the potassic zone. The alteration is distinguished by abundant sericite, pyrite, quartz, and chlorite. Propylitic alteration, developed in the host volcanic rocks, is distinguished by the occurrence of carbonates, epidote, and chlorite. A supergene argillic alteration is locally developed at surface exposures and along faults and fractures, overprinting earlier phyllic alteration.

Mineralization occurs as quartz-sulfide stockworks, as well as disseminations in the porphyritic body and the immediate volcanic host rocks, associated with both potassic and phyllic alteration types. The hypogene ore minerals include chalcopyrite and minor bornite; molybdenite is rare. Magnetite is a common constituent in the potassically altered rocks. Pyrite is common, particularly in rocks with phyllic alteration. The hypogene ore has been traced by diamond drill holes for over 500 m from surface. Some textures of mineralization are shown in Fig. 8. Supergene enrichment is irregularly developed; the enriched blanket varies in thickness from few meters to over 20 m. According to mineral assemblages and cross-cutting relationships of the veinlets and based on Gustafson and Hunt (1975) and Sillitoe (2010), the mineralization process can be roughly divided into the early, middle, and late stages

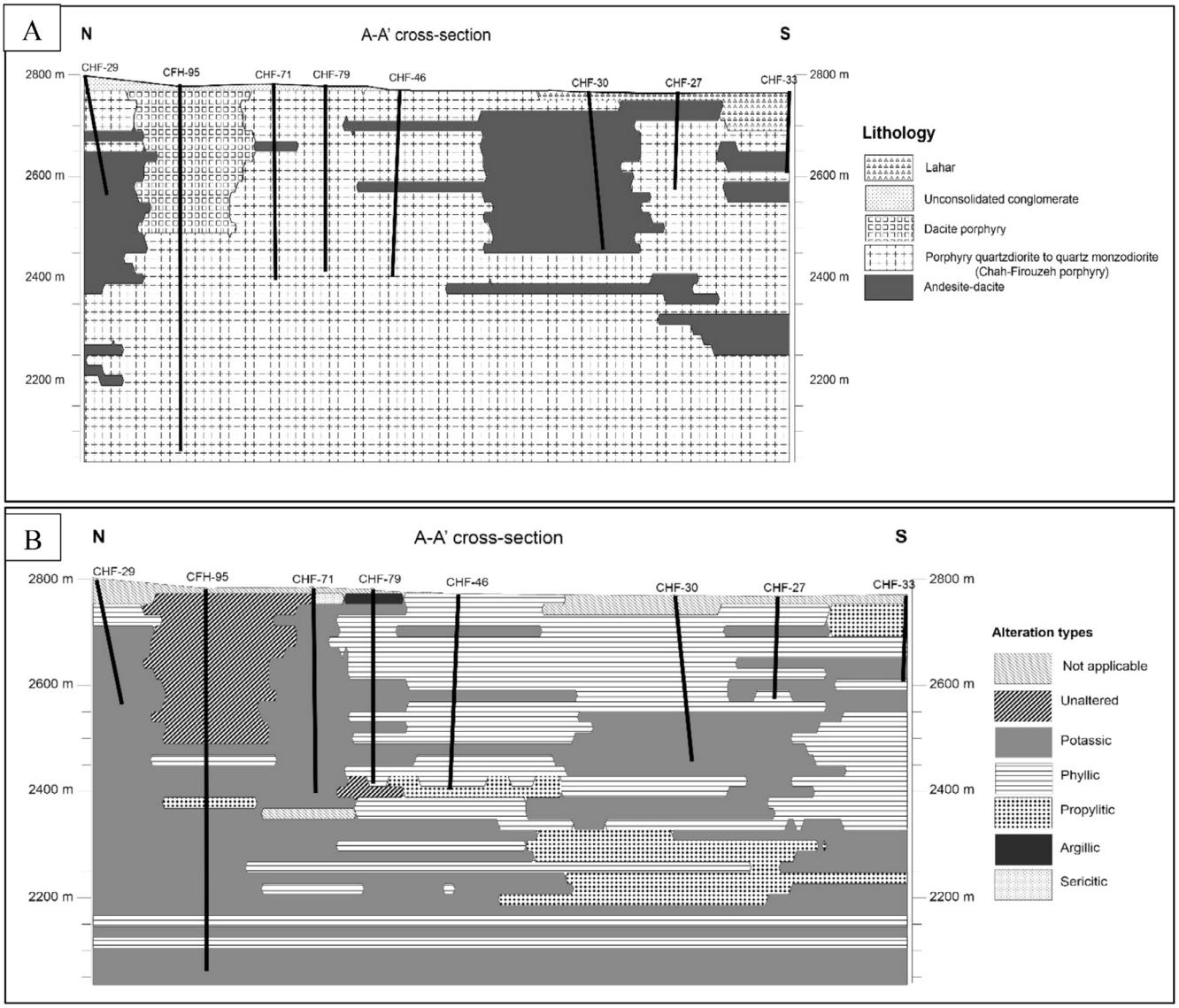

Fig. 4. North-south cross-section of the Chah-Firouzeh deposit on selected drill holes along A-A′ in Fig. 3. (A) Geological cross-section, (B) Cross-section of hydrothermal alteration patterns.

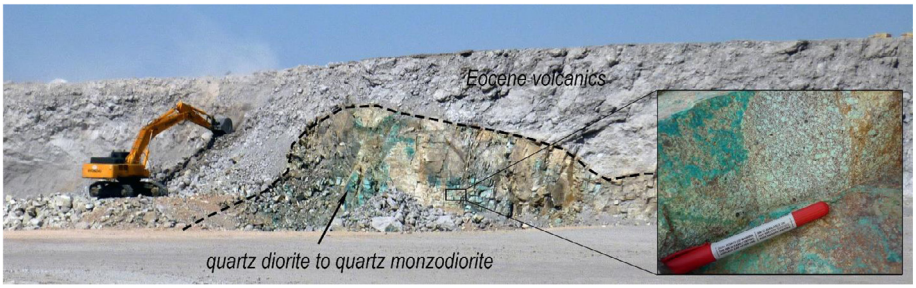

Fig. 5. The Chah-Firouzeh porphyry quartz diorite to quartz monzodiorite intruded Eocene volcanic rocks. Mineralization occurs as veinlet and stockwork system. The inset square show secondary mineralization as malachite that replaced in the fractures, as well as plagioclase phenocrysts in the Chah-Firouzeh porphyry.

producing four generations of veinlets associated with characteristic ore mineralization and wall-rock alteration (Fig. 9) The early ore-forming stage is characterized by magnetite ± actinolite (M type) and barren milky quartz to quartz ± magnetite ± chalcopyrite veinlets (A type). Anhydrite and K-feldspar can be observed in the center of some barren quartz veinlets. Narrow K-silicate envelopes are common. The middle ore-forming stage is characterized by quartz veinlets with central magnetite ± chalcopyrite ± pyrite ± chlorite ± anhydrite (B type). The sulfides in the center of veinlets show interrupted features. The late ore-forming stage is characterized by quartz ± pyrite ± chalcopyrite ± molybdenite veinlets and barren quartz veinlets with thick sericitic selvages (D type).

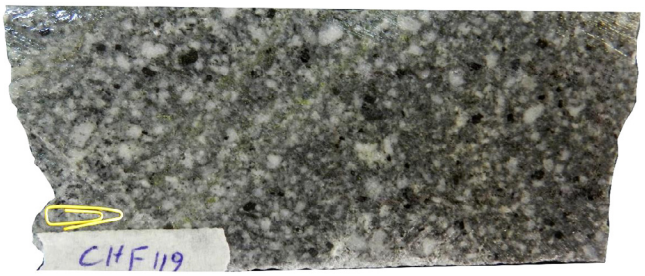

Fig. 6. Photograph of Chah-Firouzeh porphyry. Phenocrysts of quartz, plagioclase, and biotite are distributed in a fine-grained quartz-feldspar context. Borehole No. 119, depth 399 meter.

3. Sampling and analytical techniques

For zircon U–Pb geochronology, two samples representing the Chah-Firouzeh porphyry were collected from drill cores, one from borehole CHF-118, depth 60 m, the other from borehole CHF-119, depth 598 m; both boreholes drilled in the southern part of the deposit. To investigate the actual mineralization age of the Chah-Firouzeh PCD, two drill core samples with molybdenite-bearing veinlets from the hypogene ore zone were selected for Re–Os dating, one from borehole CHF-119, depth 509 m and one from borehole CHF-80, depth 609 m.

For sulfur, molybdenite, chalcopyrite, and pyrite concentrates were prepared from samples collected from "A, B, and D type" veinlets. A description of the samples is presented in Table 3. The selected minerals were crushed, washed, and then hand-picked to a purity of more than 99% under a binocular microscope.

3.1. Zircon U–Pb dating

Zircon separation from bulk samples was carried out using the mineral processing facilities available at the CSIR-National Geophysical Research Institute (CSIR-NGRI), Hyderabad, India following the mineral separation protocols mentioned in this section. About ~1 kg of drill core samples crushed by a jaw crusher and the homogenized coarse powders were ground in a steel disk mill to obtain ~80–300 μm sieve fractions. Zircon grains were concentrated by a combination of Wilfley® shaker table, Franz® isodynamic magnetic separator, methylene iodide heavy liquid, and hand picking under a binocular microscope. The zircon grains were mounted in vacuum-grade epoxy resin discs, diamond-polished and given conductive carbon coating.

Cathodoluminescence (CL) images were obtained using VEGA3 TESCAN SEM-CL at the CSIR-NGRI. The zircons were imaged at a working distance of 17 mm and accelerating voltage of 15–20 kV. The CL images were used for interpretation of internal structures manifest in spatially variable U and Th contents (Corfu et al., 2003).

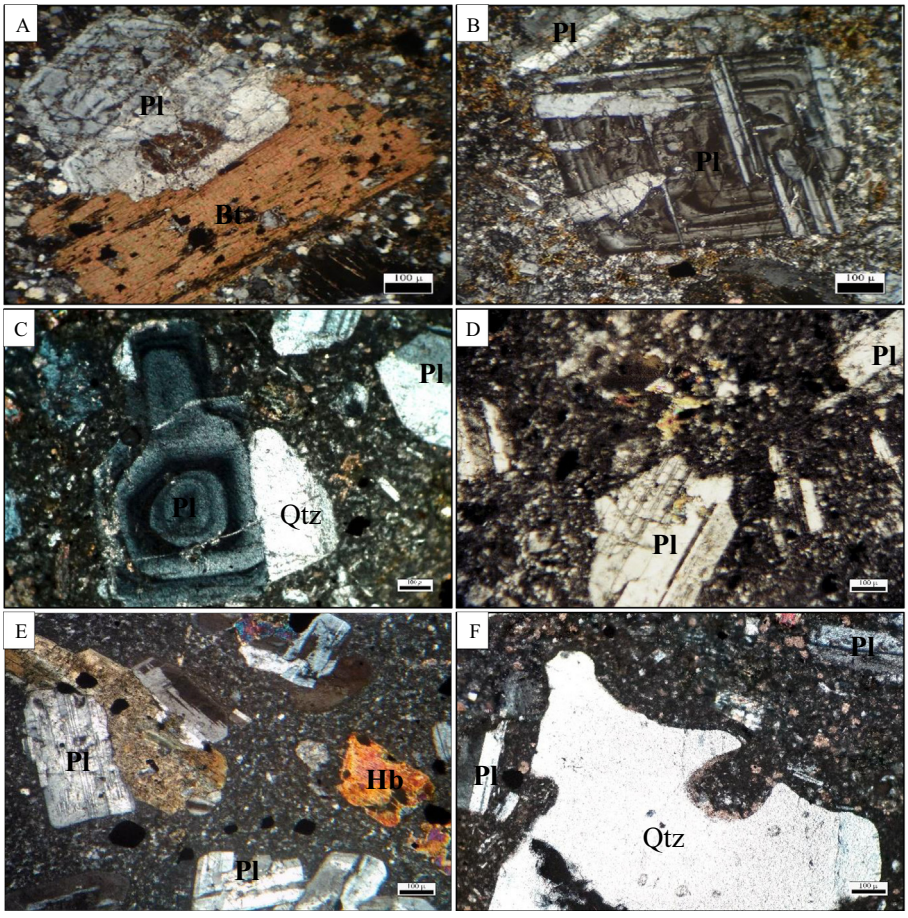

Fig. 7. Photomicrographs of various rock types in the Chah-Firouzeh deposit. All in polarized XPL light. (A and B) Chah-Firouzeh porphyry; (A) Plagioclase and biotite phenocrysts in fine quartz-feldspar groundmass. (B) Plagioclase with compositional zoning in fine quartz-feldspar groundmass. Minor secondary biotite occurs in groundmass in both samples. (C and D) Andesitic to dacitic host rock; (C) Plagioclase phenocryst shows well-developed zoning. The microcrystalline groundmass is dominated by quartz, plagioclase, and opaque minerals. (D) Plagioclase phenocrysts with polysynthetic twining in a quartz-feldspar groundmass. (E) Dioritic dyke; quartz, hornblende and biotite phenocrysts in fine-grained quartz-feldspar groundmass. (F) Young dacitic rock; resorbed quartz and plagioclase phenocrysts in a microcrystalline groundmass. Abbreviations: Bt: biotite; Hb: hornblende; Pl: plagioclase; Qtz: quartz.

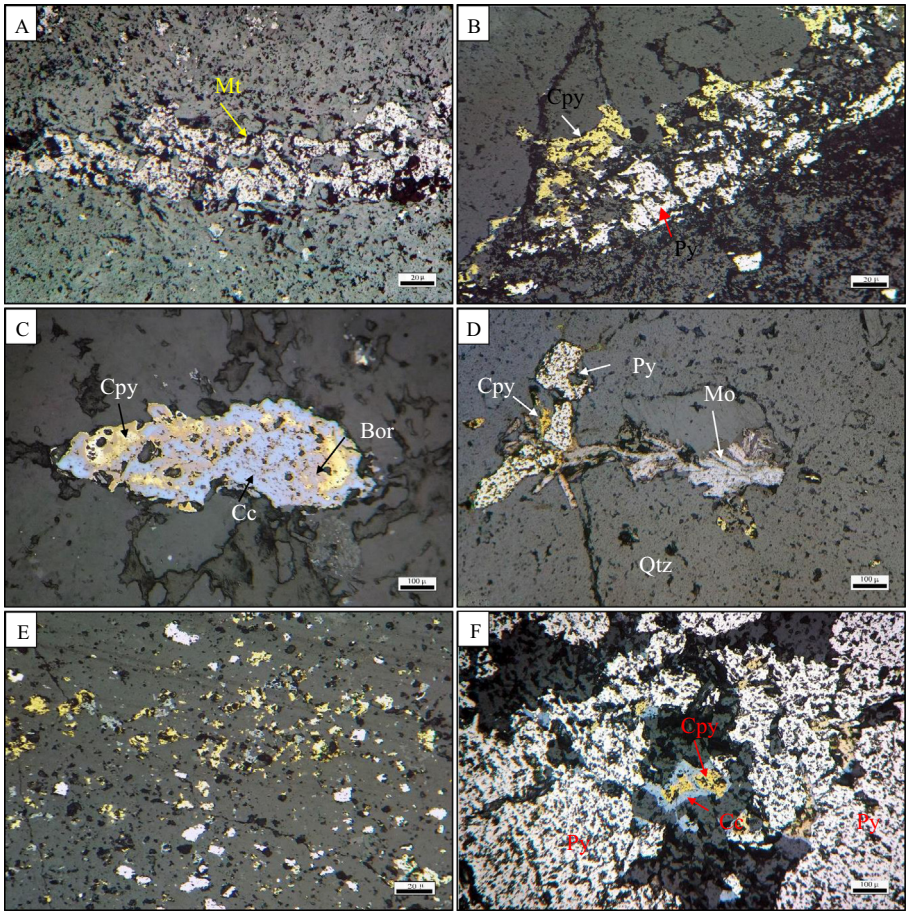

Fig. 8. Reflected light photomicrographs of selected ore textures in the Chah-Firouzeh porphyry deposit. (A) Magnetite micro-veinlet in the Chah-Firouzeh porphyry. (B) Quartz-chalcopyrite- Pyrite veinlet (B type). (C) Replacement of chalcopyrite by bornite and chalcocite. (D) Coexisting molybdenite, pyrite, and chalcopyrite in quartz veinlet. (E) Disseminated mineralization in the context of quartz monzodiorite. (F) Intergrown of pyrite and chalcopyrite. Chalcopyrite is replacing by chalcocite. Abbreviations: Bor: bornite; Cc: chalcocite; Cpy: chalcopyrite; Mo: Molybdenite; Mt: magnetite; Py: pyrite; Qtz: quartz.

U–Pb isotopic analysis was performed using an M/s New Wave Universal Platform 213 nm Nd-YAG laser ablation system coupled with M/s. Thermo X series^{II} Inductively Coupled Plasma-Mass Spectrometer (ICP-MS) at the CSIR-NGRI. A focused and continuous laser beam of 10 Hz with a diameter of 40 μm delivered fluency of 8–11 J/cm^2 to the sample and created a typical pit depth of 30–50 μm.

Each analytical session starts with a sequence commencing with two analyses of the primary zircon standard (GJ1) followed by 15 analyses of unknowns, and again followed by two analyses of primary zircon standard (GJ1) used for external standardization. The fifteen unknown analyses also include TEMORA and GJ1 zircons repeats as external reference standard for quality control purposes. Zircon reference standard GJ1, with TIMS normalizing data $^{207}Pb/^{206}Pb = 607.7 \pm 4.3$ Ma, $^{206}Pb/^{238}U = 600.7 \pm 1.1$, and $^{207}Pb/^{235}U = 602.0 \pm 1.0$ Ma (Jackson et al., 2004) was used to correct for the U–Pb fractionation and instrumental drift. The TEMORA standard U–Pb ages obtained for 7 spot analysis during this study gave a $^{206}Pb/^{238}U$ concordia age of 414 ± 10 Ma (2σ, MSWD = 5.3), which is within error of the ID-TIMS mean $^{206}Pb/^{238}U$ age of 416.00 ± 0.24 Ma determined by (Black et al., 2003) and for the standard GJ1 U–Pb ages obtained for 6 spot analysis during this study gave a $^{206}Pb/^{238}U$ Concordia age of 612 ± 9 Ma (MSWD = 0.55), demonstrating the accuracy of the operating conditions. The normalizing ages for the GJ-1 analyses over the duration of this study are $^{207}Pb/^{206}Pb = 609 \pm 4$ Ma (MSWD = 0.98), $^{206}Pb/^{238}U = 600 \pm 1$ Ma (2σ, MSWD = 2.2) and $^{207}Pb/^{235}U = 602 \pm 1$ Ma (MSWD = 1.7). U–Pb Concordia plots have been constructed using the Isoplot version 3.0 (Ludwig, 2003).

3.1.1. Samples CHF-118 and CHF-119

Two samples (CHF-118 and CHF-119) were processed for zircon extraction for the U–Pb geochronology by LA-ICP-MS at the CSIR-NGRI. SEM-CL images of zircons representing the dated samples are shown in Fig. 10. In general, zircons from the two samples display similar morphology and internal structures.

Most grains are elongated (typically 60–150 μm long with aspect ratio of 1:3) and prismatic. They show well-developed magmatic growth zoning and overall weak luminescence, similar to zircons from plutonic rocks and rare convolute zoning indicating inherited older zircon inclusions (Corfu et al., 2003). However, some grains show luminescent cores that may indicate low degrees of alteration and some grains show subrounded terminations possibly suggesting effect of magmatic resorption. Thin outer rims with brighter luminescence are often seen, interpreted here as medium U-concentration, which may indicate a reaction zone.

Sample CHF-118 (porphyry quartz diorite): U–Pb isotopic data for 17 laser spots on 17 zircon cores for the sample CHF-118 are plotted in Fig. 11. A dominant population of zircons yields a concordant age of 16.9 ± 0.4 Ma (MSWD = 0.63). The age is interpreted as the time of emplacement and magmatic crystallization.

Sample CHF-119 (porphyry quartz monzodiorite): U–Pb isotopic data for 28 laser spots on 28 zircon cores for the sample CHF-119 are plotted inFig. 11. A dominant population of concordant zircons

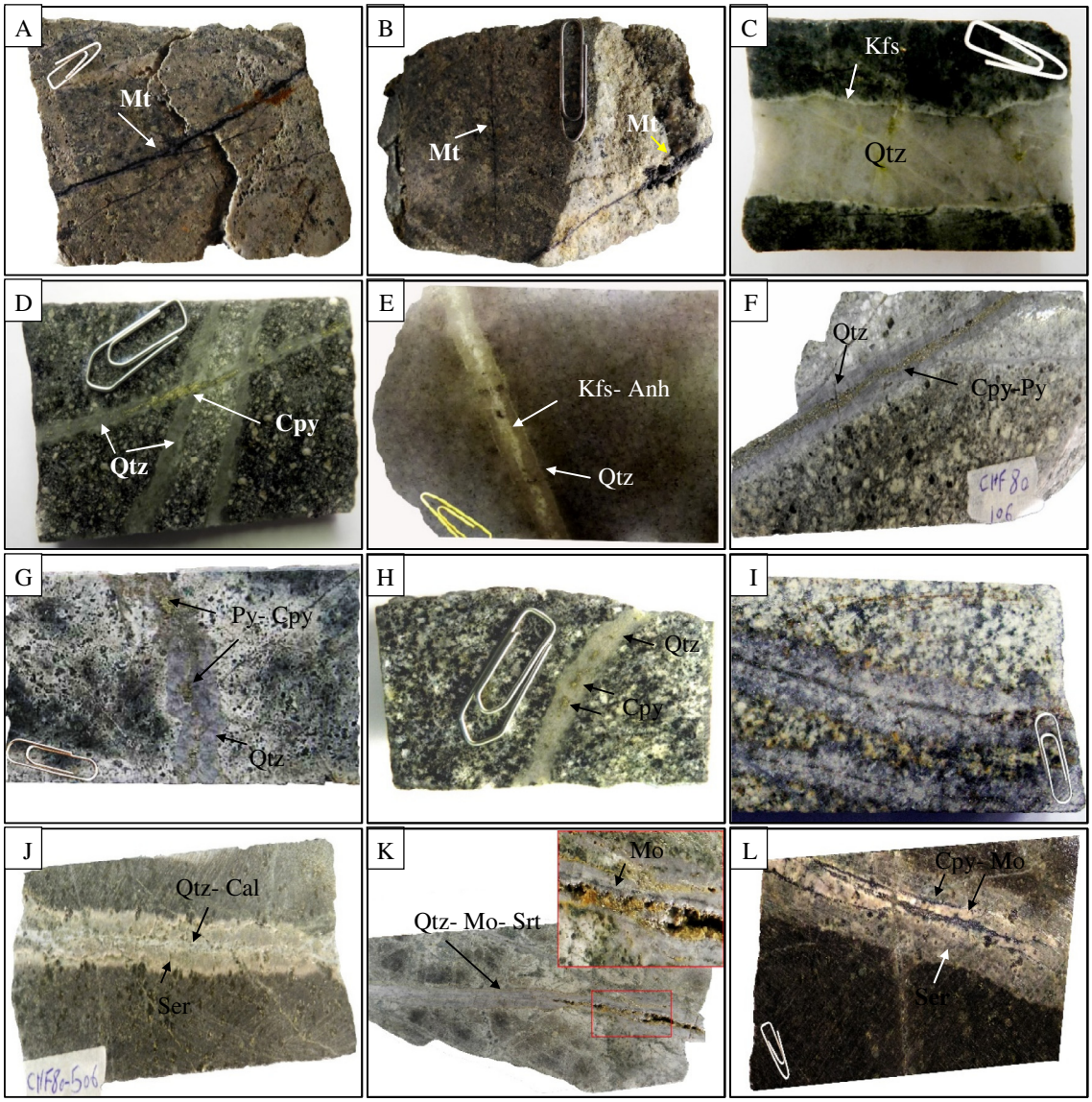

Fig. 9. Various veinlet types in the Chah-Firouzeh deposit. (A and B) Magnetite veinlet (M type) in the Chah-Firouzeh porphyry with potassic and overprinted argillic alteration. (C–E). Early stage quartz ± sulfide veinlets (A type). (F–I) Middle stage B type veinlets with irregular to sinusoidal shapes and discontinuous sulfides in the center (J–L) Late stage quartz ± carbonate ± sulfide veinlets (D type) with sericitic envelope and vuggy spaces. Abbreviations: Anh: anhydrite; Cal: calcite; Cpy: chalcopyrite; Kfs: K-feldspar; Mo: Molybdenite; Mt: magnetite; Py: pyrite; Qtz: quartz; Srt: sericite.

yields a concordant age of 16.5 ± 0.2 Ma (MSWD = 0.74). The 16.5 ± 0.2 Ma concordant age could mark the time of magmatic crystallization of the Chah-Firouzeh porphyry stock. The U–Pb data for the two samples are summarized in Table 1.

3.2. Molybdenite Re–Os dating

Re–Os dating of molybdenite provides robust primary radiometric dates as the Os in molybdenite is almost always nearly 100% radiogenic daughter ^{187}Os and the assumed value for the initial $^{187}Os/^{188}Os$ ratio has no impact on the age calculation (Stein et al., 2001; Stein, 2014 and references therein).

Two samples of molybdenite-bearing veinlets from two different drill cores were selected for Re-Os dating. Both samples had clearly visible molybdenite in low to very low abundances (Fig. 12). Sample CHF 119-509 is a "B type" veinlet in a porphyritic quartz monzodiorite and includes quartz and molybdenite. Sample CHF 80-609 is a vuggy, late stage "D type" veinlet in a porphyritic quartz monzodiorite host. Vugs are in the range of cm size, and mineral assemblage includes quartz + calcite + pyrite + chalcopyrite, and molybdenite. The chalcopyrite displays conchoidal fractures and crystal faces in vugs; pyrite is relatively scarce; molybdenite is abundant throughout the veinlet as very fine-grained clusters and disseminated in a drusy matrix of quartz-late carbonate (Fig. 12).

Molybdenite mineral separates were acquired using a small hand-held drill, with the aim of collecting the distinct occurrences of the mineral in the veinlet and rock context. Re–Os analyses were carried out using a mixed Re-double Os spike (Markey et al., 2003). Concentrations were determined by measuring isotopic ratios using NTIMS on a Triton instrument at the AIRIE Program, Colorado State University. The Re–Os isotopic data and ages are presented in Table 2.

3.3. Sulfur isotopes

Sulfur isotope ratios were measured on an IsoPrime100 stable isotope ratio mass spectrometer (IRMS) at the Guangzhou Institute

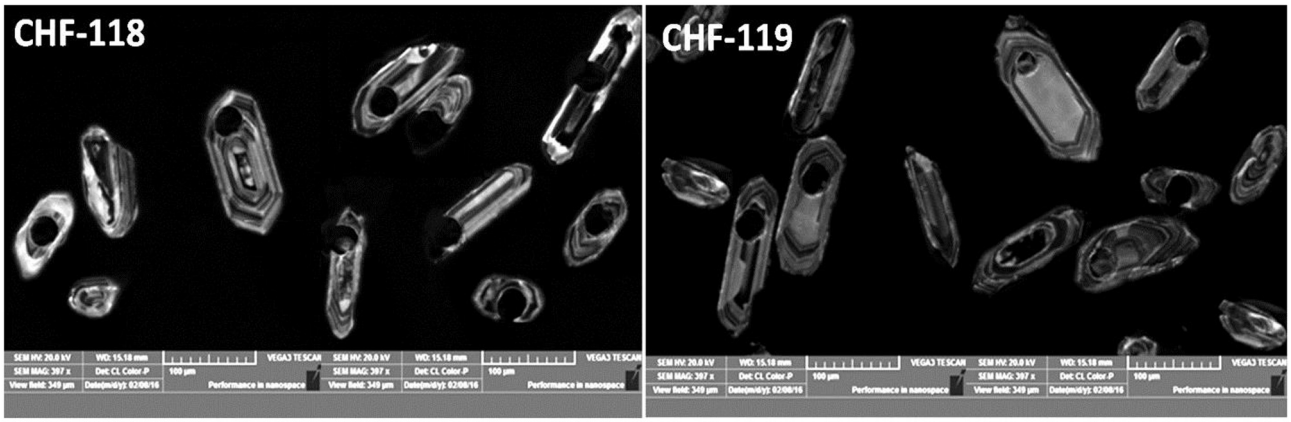

Fig. 10. Cathodoluminescence images showing morphological features of representative zircon grains of the Chah-Firouzeh porphyry, analyzed by LA-ICP-MS.

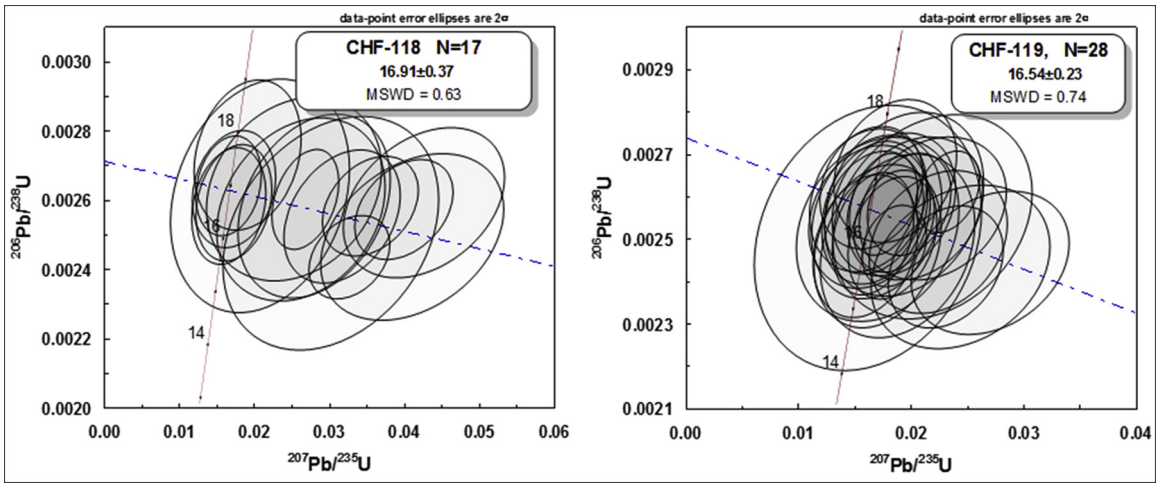

Fig. 11. Zircon U–Pb Concordia diagrams for Chah-Firouzeh porphyry stock.

of Geochemistry, Chinese Academy of Sciences, Guangzhou, China. Thirteen samples from various types of quartz-sulfide veinlets of hypogene zone were selected for sulfur isotope analysis. Sulfur isotope analysis was performed on pyrite, chalcopyrite, and molybdenite. A description of the samples and the $\delta^{34}S$ values are presented in Table 3. The $\delta^{34}S$ values in the potassic zone vary from −1.3 to +0.7‰ with an average value of −0.04‰; in the overprinted phyllic-potassic zone is between −0.7 and +0.8‰ with an average value of +0.17‰ and in the phyllic zone is from −1.4 to +2.5‰ with an average value of +0.9‰.

4. Discussion

4.1. Geochronology

Our new zircon U–Pb geochronological data suggest crystallization age between 16.91 ± 0.37 Ma and 16.54 ± 0.23 Ma, and confirms that the Chah-Firouzeh porphyry stock was emplaced in the early-middle Miocene. The two selected samples for U–Pb dating offer close overlap, and just have 0.35 m.y. duration. This suggests that the Chah-Firouzeh porphyry stock was probably emplaced during one stage and cooled slowly and uniformly through the zircon closure temperature.

Based on zircon U–Pb dating in the Meiduk cluster (Hassanzadeh, 1993; McInnes et al., 2003, 2005; Mirnejad et al., 2013; Aghazadeh et al., 2015), porphyry granitoids emplaced approximately at short intervals from middle to late Miocene in this region. Chah-Firouzeh porphyry stock with 16.91 ± 0.37 Ma age is the oldest intrusive body and Abdar prospect with 7.3 ± 0.3 Ma (McInnes et al., 2003) is the youngest one (Table 4 and Fig. 13) suggesting at least ~ 9.6 m.y. plutonism in the Meiduk cluster.

This indicates that during the Miocene, magmatism was strongly active in NW part of KCMA and magma emplacement continuously occurred in several episodes over about ~9.6 m.y. It should also be considered that there are some intrusive bodies in the Meiduk cluster that have not been dated yet and likely formed during this time frame.

During middle-late Miocene, a post-collisional tectonic regime was dominant in the KCMA (Shafiei et al., 2009; Dargahi et al., 2010; Aghazadeh et al., 2015) and shallow level plutons with adakitic nature (Kuh Panj type granitoids) were emplaced and formed the most important porphyry mineralization stage in the KCMA (Shafiei, 2008, 2010; Shafiei et al., 2009; Asadi et al., 2014; Aghazadeh et al., 2015). Results of the current research reveal that the Chah-Firouzeh porphyry deposit as the oldest member of the Meiduk cluster, emplaced at the beginning stage of the post-collisional geodynamic regime and adakitic magma generation. This deposit represents the earliest piece of continuous magma emplacement sequence in time and space, along with several other large and small granitoid plutons formed an important Cu porphyry metallogenic region in the northwestern part of KCMA.

Table 1
Laser Ablation ICP-MS U-Th-Pb isotopic data and calculated ages for zircons from the Chah-Firouzeh porphyry stock.

Analysis_#	Th ppm	U ppm	Th/U	$^{207}Pb/^{235}U$	2σ	$^{206}Pb/^{238}U$	2σ	rho	$^{207}Pb/^{206}Pb$	1σ	$^{206}Pb/^{238}U$	1σ
Sample CHF-118												
CHF-118-01	14.6	26.5	0.55	0.04095	0.00992	0.00249	0.0002	0.33	16.1	0.64	40.7	4.84
CHF-118-02	11.9	22.7	0.53	0.01733	0.00452	0.00263	0.00014	0.20	16.9	0.48	17.4	2.26
CHF-118-03	32.2	51.4	0.63	0.01661	0.00354	0.00264	0.00012	0.21	17	0.41	16.7	1.77
CHF-118-04	14.7	25.5	0.58	0.02077	0.0097	0.00261	0.00028	0.23	16.8	0.92	20.9	4.82
CHF-118-05	11.3	28.2	0.40	0.04252	0.00876	0.00259	0.00018	0.34	16.7	0.57	42.3	4.26
CHF-118-06	58.1	70.9	0.82	0.03261	0.00438	0.00243	0.0001	0.31	15.7	0.35	32.6	2.15
CHF-118-07	21.3	25.9	0.82	0.01915	0.0058	0.00273	0.00018	0.22	17.6	0.59	19.3	2.89
CHF-118-08	63.7	84.4	0.75	0.02677	0.0036	0.0026	0.00012	0.34	16.7	0.35	26.8	1.78
CHF-118-09	7.0	14.5	0.48	0.02618	0.00914	0.00257	0.00022	0.25	16.5	0.74	26.2	4.52
CHF-118-10	40.7	35.4	1.15	0.02796	0.00826	0.00258	0.00022	0.29	16.6	0.68	28	4.08
CHF-118-11	5.8	9.8	0.59	0.02528	0.0095	0.00263	0.00022	0.22	17	0.73	25.3	4.7
CHF-118-12	24.0	42.4	0.57	0.03542	0.00518	0.00258	0.00012	0.32	16.6	0.41	35.3	2.54
CHF-118-13	28.9	38.8	0.75	0.03167	0.00628	0.00255	0.00016	0.32	16.4	0.49	31.7	3.09
CHF-118-14	7.9	15.6	0.51	0.03017	0.01168	0.0025	0.00028	0.29	16.1	0.89	30.2	5.76
CHF-118-15	42.2	54.3	0.78	0.01662	0.00402	0.00258	0.00014	0.22	16.6	0.47	16.7	2.01
CHF-118-16	56.7	43.9	1.29	0.01729	0.00412	0.00259	0.00014	0.23	16.7	0.45	17.4	2.06
CHF-118-17	108.5	95.2	1.14	0.03985	0.00536	0.00257	0.00012	0.35	16.5	0.39	39.7	2.61
Sample CHF-119												
CHF-119-01	6.3	19.2	0.33	0.0162	0.00424	0.00259	0.00014	0.21	16.7	0.45	16.3	2.12
CHF-119-02	14.7	28.2	0.52	0.01677	0.00384	0.00256	0.00014	0.24	16.5	0.43	16.9	1.91
CHF-119-03	25.8	34.8	0.74	0.01596	0.0038	0.00248	0.00014	0.24	16	0.42	16.1	1.89
CHF-119-04	16.4	27.0	0.61	0.01849	0.00292	0.00254	0.0001	0.25	16.4	0.32	18.6	1.46
CHF-119-05	12.5	20.1	0.62	0.02305	0.00414	0.00243	0.00012	0.27	15.6	0.37	23.1	2.06
CHF-119-06	19.5	29.3	0.67	0.01937	0.00574	0.00258	0.00018	0.24	16.6	0.55	19.5	2.86
CHF-119-07	25.1	38.2	0.66	0.01879	0.00558	0.00248	0.00018	0.24	16	0.56	18.9	2.78
CHF-119-08	76.8	72.8	1.05	0.01664	0.00296	0.00251	0.00012	0.27	16.2	0.35	16.8	1.48
CHF-119-09	24.1	41.8	0.58	0.02698	0.0057	0.00244	0.00014	0.27	15.7	0.48	27	2.81
CHF-119-10	17.3	33.2	0.52	0.01649	0.00372	0.00262	0.00012	0.20	16.9	0.41	16.6	1.86
CHF-119-11	14.1	28.4	0.50	0.01616	0.0082	0.0025	0.00026	0.20	16.1	0.83	16.3	4.1
CHF-119-12	14.5	22.4	0.65	0.02435	0.00646	0.00243	0.00016	0.25	15.6	0.54	24.4	3.21
CHF-119-13	10.3	16.7	0.62	0.02188	0.0072	0.00255	0.0002	0.24	16.4	0.64	22	3.57
CHF-119-14	31.1	33.2	0.94	0.01833	0.00322	0.0025	0.00012	0.27	16.1	0.35	18.4	1.61
CHF-119-15	13.8	30.4	0.45	0.01632	0.00438	0.00255	0.00014	0.20	16.4	0.47	16.4	2.19
CHF-119-16	14.2	22.3	0.64	0.02032	0.0049	0.00257	0.00014	0.23	16.5	0.47	20.4	2.44
CHF-119-17	12.6	27.6	0.46	0.01696	0.00468	0.00255	0.00016	0.23	16.4	0.5	17.1	2.34
CHF-119-18	6.5	14.3	0.45	0.01701	0.00586	0.00252	0.00018	0.21	16.2	0.58	17.1	2.92
CHF-119-19	34.7	46.6	0.75	0.02324	0.0023	0.00261	0.00008	0.31	16.8	0.26	23.3	1.14
CHF-119-20	26.7	37.7	0.71	0.01756	0.00246	0.00258	0.0001	0.28	16.6	0.29	17.7	1.23
CHF-119-21	42.2	66.1	0.64	0.01852	0.00234	0.00248	0.00008	0.26	16	0.28	18.6	1.16
CHF-119-22	21.2	44.5	0.48	0.01846	0.00446	0.00258	0.00014	0.22	16.6	0.47	18.6	2.22
CHF-119-23	17.5	28.3	0.62	0.0219	0.0053	0.00257	0.00014	0.23	16.5	0.48	22	2.63
CHF-119-24	27.9	45.1	0.62	0.01859	0.00442	0.00266	0.00014	0.22	17.1	0.47	18.7	2.2
CHF-119-25	36.7	58.0	0.63	0.01672	0.00358	0.00256	0.00012	0.22	16.5	0.41	16.8	1.78
CHF-119-26	10.7	30.4	0.35	0.02237	0.00498	0.00249	0.00014	0.25	16	0.45	22.5	2.47
CHF-119-27	18.8	35.5	0.53	0.01984	0.00302	0.00258	0.0001	0.25	16.6	0.33	19.9	1.5
CHF-119-28	15.7	36.8	0.43	0.01702	0.00458	0.00248	0.00016	0.24	16	0.48	17.1	2.28

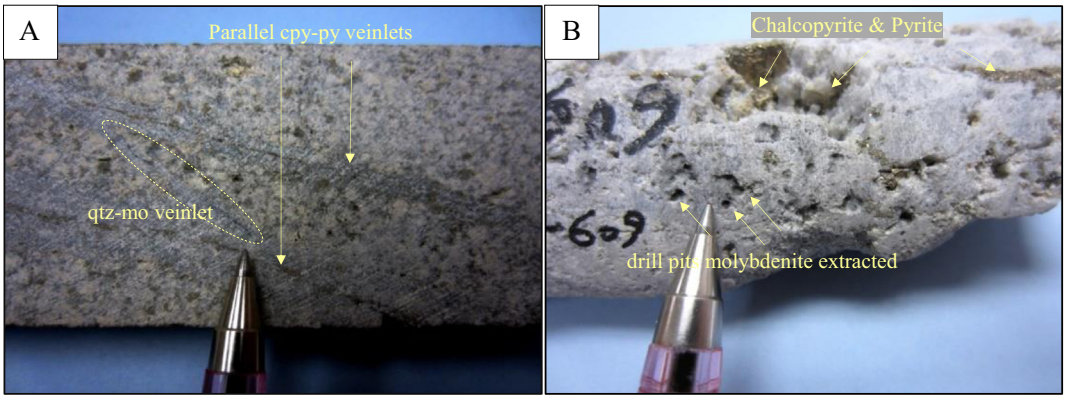

Fig. 12. Photographs of drill cores sampled for molybdenite. (A) Sample (CHF 119-509), typical "B type" vein in porphyritic quartz monzonite (Chah-Firouzeh porphyry) including abundant disseminated pyrite in the rock context. Earlier potassic alteration overprinted by strong phyllic alteration. The hairline quartz-molybdenite veinlet cut by two subparallel chalcopyrite-pyrite veinlets (B) Sample (CHF 80-609), vuggy "D type" vein with quartz + pyrite + chalcopyrite + molybdenite. In porphyritic quartz monzonite host with phyllic alteration overprinted by argillic alteration. Molybdenite is abundant throughout the core piece as very fine grained clusters disseminated in a drusy matrix of quartz late carbonate. Chalcopyrite displays conchoidal fractures and crystal faces in vugs, and pyrite is rare.

Table 2
Molybdenite Re–Os data from the Chah-Firouzeh porphyry Cu deposit.

Sample	AIRIE Run #	Re, (ppm)	Re err, abs (ppm)	^{187}Os, (ppb)	^{187}Os err, abs (ppb)	OsC, (ppb)	OsC err, abs (ppb)	Age, (Ma)	Age err, abs, w/λ (Ma)	Age err, abs, analytical only (Ma)
CHF 119-509	MD-1611	115.90	0.20	20.148	0.007	0.015	0.002	16.60	0.060	0.029
CHF 80-609	MD-1612	69.15	0.11	11.580	0.006	0.001	0.001	15.99	0.058	0.027

Re–Os data acquired by Carius tube dissolution and sample equilibration with a double Os spike for mass fractionation and determination of common Os.
Sample weights are 9 mg (MD-1611) and 22 mg (MD-1612); both samples are optimally spiked; samples run by NTIMS (Triton) at AIRIE Program, Colorado State University.
For MD-1611 estimated molybdenite is 20%, for MD-1612 also 20% with 10% chalcopyrite in the 80% dilution fraction (though no common Os added).
Re blank = 0.56 ± 0.02 pg, Os blank = 0.122 ± 0.005 pg with ^{187}Os/^{188}Os = 0.550 ± 0.009; blanks are completely insignificant to age calculation.
All data are reported at two-sigma uncertainty; using analytical error, the two Re–Os ages are distinct in time.

Table 3
Sulfur isotope composition of sulfides for various vein types from the Chah-Firouzeh porphyry Cu deposit.

Sample	Vein type	Assemblage	Alteration	Analyzed Mineral	δ^{34}S (‰, CDT)	Mineral pair T (°C)
CHF 80-S1	B vein type	Qtz + Py + Cpy + Mo + Anh	Potassic	Molybdenite	−1.3	
CHF 80-S2	B vein type	Qtz + Py + Cpy + Mo + Anh	Potassic	Pyrite	0.2	881[a]
CHF 80-S3	B vein type	Qtz + Py + Cpy + Mo + Anh	Potassic	Chalcopyrite	0.5	
CHF 80-S4	D vein type	Qtz + Py	Potassic	Pyrite	0.7	
CHF 80-S5	A vein type	Qtz + Mag + Py	Potassic	Pyrite	−0.3	
CHF 118-S6	A vein type	Qtz + Mag + Py	Phyllic	Pyrite	1.1	
CHF 118-S7	B vein type	Qtz + Py + Cpy	Phyllic	Chalcopyrite	−1.4	
CHF 118-S8	A vein type	Qtz + Mag + Py + Cpy	Phyllic	Pyrite	1.4	329[a]
CHF 118-S9	A vein type	Qtz + Mag + Py + Cpy	Phyllic	Chalcopyrite	2.5	
CHF 119-S10	B vein type	Qtz + Py + Mo + Cpy	Phyllic-Potassic	Pyrite	−0.7	
CHF 119-S11	B vein type	Qtz + Py + Mo + Cpy	Phyllic-Potassic	Chalcopyrite	0.1	535[b]
CHF 119-S12	B vein type	Qtz + Py + Mo + Cpy	Phyllic-Potassic	Molybdenite	0.5	
CHF 119-S13	D vein type	Qtz + Py	Phyllic-Potassic	Pyrite	0.8	402[b]

Sulfur isotope thermometers according to: a) Ohmoto and Rye (1979), b) Suvorova (1974).
Mineral abbreviations: Anh = anhydrite, Cpy = chalcopyrite, Mag = magnetite, Mo = molybdenite, Py = pyrite, Qtz = quartz.

Table 4
Published geochronological data for the Meiduk cluster porphyry copper deposits and prospects.

Deposit	Description	Analyzed Mineral	Method	Age (Ma)	Reference
Meiduk	Meiduk porphyry	Zircon	U–Pb	12.5 ± 0.1	McInnes et al. (2003)
	Meiduk porphyry	Zircon	U-Th/He	12.5 ± 0.5	McInnes et al. (2003)
	Meiduk porphyry	Zircon	U–Pb	12 ± 0.8	Aghazadeh et al. (2015)
	Meiduk porphyry	Zircon	U–Pb	10.8 ± 0.5	Aghazadeh et al. (2015)
	Meiduk porphyry	Apatite	U-Th/He	9.5	McInnes et al. (2003)
	Potassic alteration	Whole rock	Rb-Sr (3 point isochron)	12.4 ± 4.5	Hassanzadeh (1993)
	Potassic alteration	Biotite	Ar-Ar	11.2 ± 0.5	Hassanzadeh (1993)
	Potassic alteration	K-feldspar	Ar-Ar	11.2 ± 0.4	Hassanzadeh (1993)
	Phyllic alteration	Sericite	Ar-Ar	10.8 ± 0.4	Hassanzadeh (1993)
	Mineralized vein	Molybdenite	Re-Os	12.36 ± 0.07	Taghipour et al. (2008)
	Disseminated molybdenite Flakes within anhydrite from P2 porphyry	Molybdenite	Re-Os	12.10 ± 0.07	Taghipour et al. (2008)
Chah-Firouzeh	**Chah-Firouzeh porphyry**	**Zircon**	**U–Pb**	**16.91 ± 0.37**	**This study**
	Chah-Firouzeh porphyry	**Zircon**	**U–Pb**	**16.54 ± 0.23**	**This study**
	Mineralized vein	**Molybdenite**	**Re-Os**	**16.60 ± 0.06**	**This study**
	Mineralized vein	**Molybdenite**	**Re-Os**	**15.99 ± 0.06**	**This study**
	Mineralized vein	Molybdenite	Re-Os	16.19 ± 0.23	Aghazadeh et al. (2015)
Iju	Iju Porphyry	Zircon	U–Pb	9.2 ± 0.1	McInnes et al. (2003)
	Iju porphyry	Zircon	U–Pb	9.27 ± 0.5	Mirnejad et al. (2013)
	Iju porphyry	Zircon	U-Th/He	10.9 ± 0.4	McInnes et al. (2003)
	Mineralized vein	Molybdenite	Re-Os	9.8 ± 0.06	Mirnejad et al. (2013)
	Mineralized vein	Molybdenite	Re-Os	9.24 ± 0.14	Aghazadeh et al. (2015)
	Mineralized vein	Molybdenite	Re-Os	9.03 ± 0.13	Aghazadeh et al. (2015)
Abdar	Abdar diorite subvolcanic	Zircon	U–Pb	7.5 ± 0.1	McInnes et al. (2003)
	Abdar diorite subvolcanic	Zircon	U-Th/He	7.3 ± 0.3	McInnes et al. (2003)
	Potassic alteration	Apatite	U-Th/He	4.9 ± 0.4	McInnes et al. (2003)
	Lava flows*	Biotite	Ar-Ar	6.8 ± 0.4	Hassanzadeh (1993)
	Lava flows*	Hornblende	Ar-Ar	6.4 ± 0.8; 6.3 ± 0.9	Hassanzadeh (1993)
	Mineralized vein	Molybdenite	Re-Os	6.41 ± 0.26	Aghazadeh et al. (2015)
	Mineralized vein	Molybdenite	Re-Os	6.19 ± 0.1	Aghazadeh et al. (2015)
Kader	**Kader porphyry**	**Zircon**	**U–Pb**	**7.54 ± 0.15**	**Mohammaddoost**
	Kader porphyry	**Zircon**	**U–Pb**	**7.47 ± 0.25**	**Unpublished data**
Serenu	**Serenu porphyry**	**Zircon**	**U–Pb**	**10.20 ± 0.17**	**Mohammaddoost**
	Serenu porphyry	**Zircon**	**U–Pb**	**9.83 ± 0.4**	**Unpublished data**
Gode-Kolvari	**Gode-Kolvari porphyry**	**Zircon**	**U–Pb**	**16.36 ± 0.37**	**Mohammaddoost**
	Gode-Kolvari porphyry	**Zircon**	**U–Pb**	**15.04 ± 14**	**unpublished data**

* Lava flows on flanks of Kuh-e-Masahim volcano that surrounded the Abdar diorite intrusion.

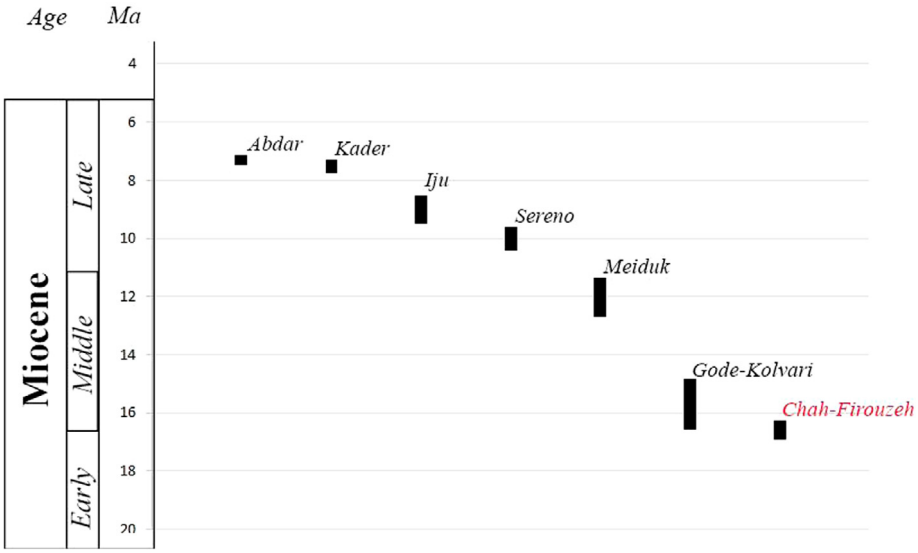

Fig. 13. Emplacement model of Meiduk cluster porphyry granitoids, based on zircon U-Pb dating. Chah-Firouzeh deposit was emplaced in the early-middle Miocene.

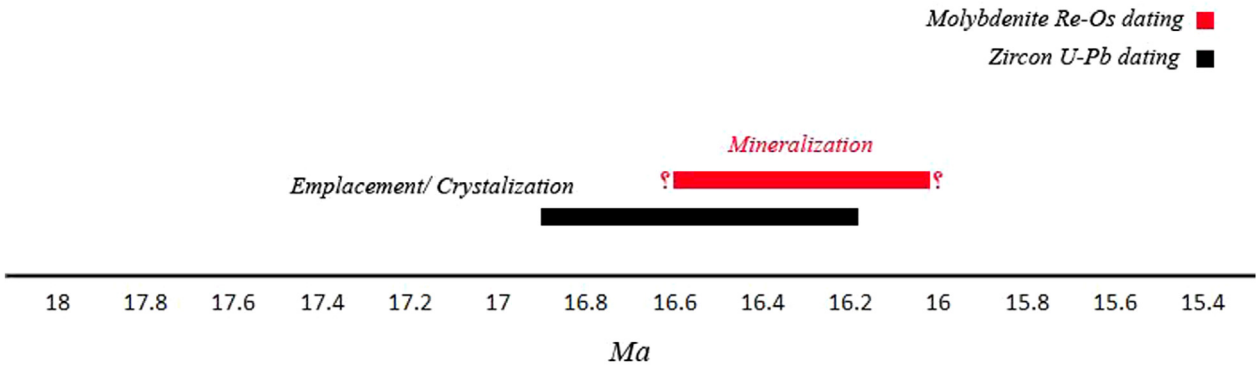

Fig. 14. Age of magma emplacement versus mineralization in the Chah-Firouzeh porphyry copper deposit; Molybdenite Re–Os dating reveals that duration of mineralization was at least 600,000 years. Comparing the zircon U–Pb and molybdenite Re–Os results suggests that mineralization was contemporaneous with final stage of magma emplacement, and continued afterwards.

Linking between emplacement/crystallization versus mineralization age in porphyry deposits has been studied by many authors applying U–Pb and Re–Os systematics to provide information on magma emplacement history, subsequent events, and their duration (e.g., Torrealday et al., 2000; Valencia et al., 2006; Selby et al., 2007; Pankhurst et al., 2013; Del Rio-Salas et al., 2015; Wang et al., 2015). There have recently been examples of studies by some researchers using this method for reconstructing the time duration between magma emplacement and mineralization for some PCDs from Iran (e.g., Mirnejad et al., 2013; Aghazadeh et al., 2015).

The Re–Os ages are slightly younger than U–Pb zircon ages and have overlap within error with the U–Pb age of the Chah-Firouzeh porphyry host rock. The two Re–Os ages represent two different mineralizing episodes, based on analytical errors (16.60 ± 0.06 Ma and 15.99 ± 0.06 Ma for CHF 119 and CHF 80, respectively). Even with the full error, the two Re–Os ages still do not quite overlap at the two-sigma level. These two ages suggest that the duration of mineralization was at least ~0.6 million years, and almost certainly longer, as it is highly unlikely that we captured the oldest and youngest events in just two samples. Aghazadeh et al. (2015) reported an age of 16.19 ± 0.23 Ma for the Chah-Firouzeh deposit.

Investigation on the other PCDs in the Meiduk cluster suggests similar lifespans for mineralization (Table 4) (Fig. 15). Main stage mineralization at the Iju deposit lasted over ~770,000 years, and at the Abdar deposit over ~220,000 years. Molybdenite Re-Os dating on two samples from the Meiduk deposit (Taghipour et al., 2008) indicates ~260,000 years for mineralization lifespan, but considering that probably the samples were taken from the same mineralization stage, the true lifetime is likely longer. Given that at least two phases of magma intrusion occurred in the Meiduk deposit (Taghipour et al., 2008), the fluid generation and mineralization duration can be over a million years. Regarding the Ar-Ar dating of potassic and phyllic alteration types (Hassanzadeh, 1993) (Table 4), the mineralization lifespan in the Meiduk is likely over ~1.6 million years. Thus, on the district-scale, PCD mineralization in the Meiduk cluster varied from ~0.2 to 1.6 m.y. with an average of ~0.8 m.y. These are minimum lifespans, because the dated samples most probably are not representative of the oldest and youngest events of mineralization. However, this indicates that fundamental magmatic-hydrothermal processes leading to porphyry mineralization in the Meiduk cluster were fast and short-lived.

It is estimated that the lifetime of hydrothermal activity associated with porphyry deposits to be a few hundred thousand years

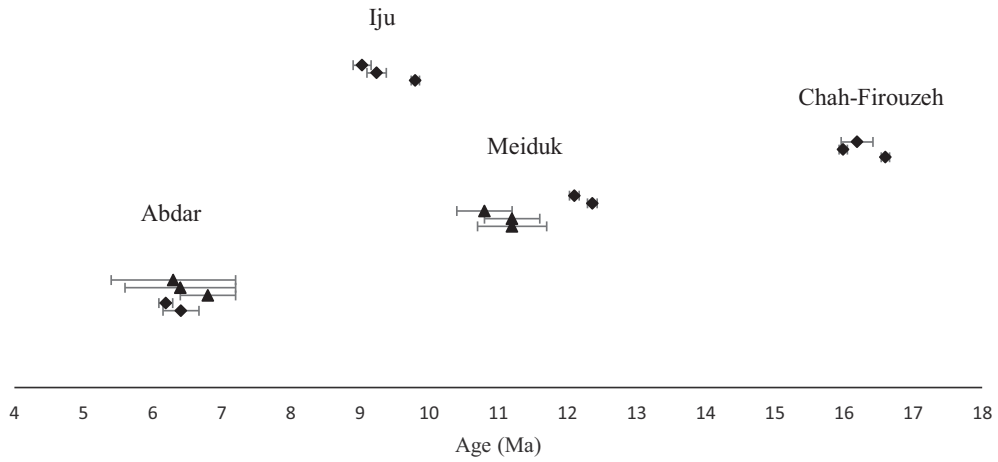

Fig. 15. Re–Os and Ar-Ar ages of PCDs in the Meiduk cluster (references in text). Ore mineralization occurs in 0.2–1.6 m.y., indicating rapid magmatic-hydrothermal processes on the deposit scale.

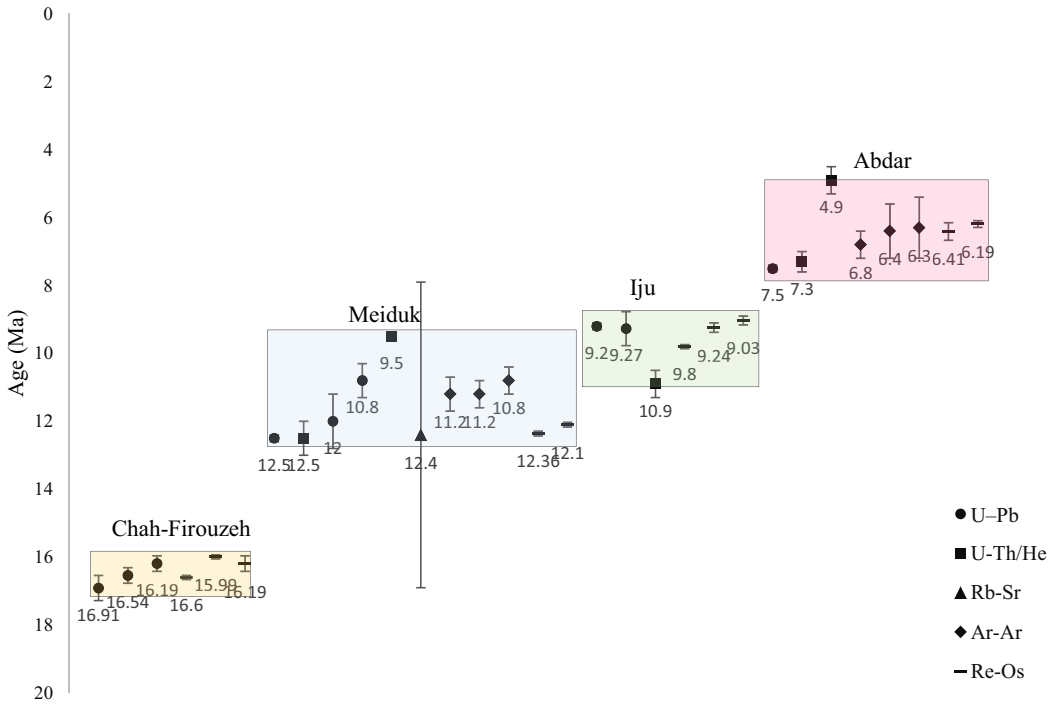

Fig. 16. Reconstruction model of emplacement/crystallization and duration of hydrothermal activity and mineralization based on geochronological data at the Chah-Firouzeh, Meiduk, Iju, and Abdar deposits. Geochronological data from Hassanzadeh (1993), McInnes et al. (2003), Taghipour et al. (2008), Mirnejad et al. (2013), Aghazadeh et al. (2015) and this study.

(Marsh et al., 1997; Zimmerman et al., 2008, 2014; Von Quadt et al., 2011). Although the duration of a magmatic hydrothermal system depends on several factors, numerical modeling studies suggest about 800,000 years of duration for a single intrusion under optimal conditions (Cathles et al., 1997). For multiple intrusions, this lifetime can increase to more than 1 million years (John et al., 2010).

Comparing the zircon U–Pb and molybdenite Re–Os results for the Chah-Firouzeh (Fig. 14) reveals that during crystallization of the intrusion, the hydrothermal ore deposition started. The mineralization was going on simultaneous with middle stage of magma crystallization, when sufficient volumes of volatiles and ore-forming fluids exsolved from a crystallizing magma. The ore deposition continued after magma crystallization and with the onset of cooling process, meteoric fluids increased slowly in the system and mineralization continued with influx of meteoric fluids.

Re-compiling geochronological data for other deposits/prospects of the Meiduk cluster (Table 4) demonstrates that the post-collisional tectonic regime in NW part of KCMA was relatively fast, so that porphyry deposit formation occurred in a few hundred thousand years pulses during a ~9.6 m.y. tectonic framework. As well as there is a short duration between magma emplacement and beginning of hydrothermal process and mineralization in the porphyry deposits in this area (Fig. 16). For example, mineralization in the Meiduk deposit is contemporaneous with P2 porphyry emplacement (Taghipour et al., 2008) and also for Iju deposit and Abdar prospect, mineralization started simultaneous with middle stage of magma crystallization.

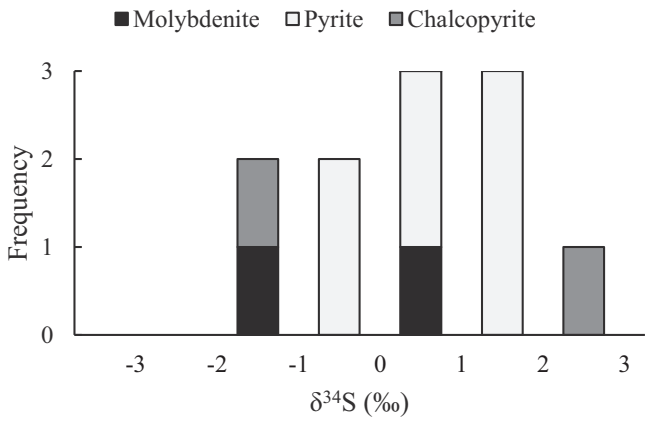

Fig. 17. Histogram showing the sulfur isotope data from Chah-Firouzeh deposit.

McInnes et al. (2003) note that magma emplacement close to the surface and uplift during Miocene collision and post-collision compression and consequent rapid cooling due to shallow level exhumation, play an important role in formation of porphyry deposits in the Meiduk cluster.

4.2. Sulfur isotope ratios

The $\delta^{34}S$ values of sulfide minerals from the Chah-Firouzeh deposit exhibit a narrow range of −1.4 to +2.5‰ (Fig. 17) consistent with the $\delta^{34}S$ values of sulfide minerals reported from many porphyry deposits worldwide (Allègre, 2008) and suggest a homogeneous hydrothermal system in which the sulfur is related to a magmatic source. The $\delta^{34}S$ values have a uniform range near zero and no significant differences in $\delta^{34}S$ values can be distinguished between various vein types.

The $\delta^{34}S$ values of sulfide minerals in PCDs generally range from −5 to +5‰, which is the accepted range for magmatic water (Ohmoto and Rye, 1979; Allègre, 2008). The $\delta^{34}S$ values of some PCDs in the KCMA, such as Iju, Darreh-Zar, and Meiduk fall in this range (Taghipoor, 2007; Mirnejad et al., 2013; Parsapoor et al., 2014). Temperatures calculated from the isotopic composition of coexisting sulfide pairs are consistent with the temperatures measured from fluid inclusions, implying sulfide deposition under equilibrium isotopic conditions.

Calculation of isotope equilibrium temperature for sulfide pairs, using the $\Delta^{34}S_{py\text{-}cpy}$, $\Delta^{34}S_{Mo\text{-}cpy}$, and $\Delta^{34}S_{Mo\text{-}cpy}$ values, produce temperatures from 329 to 881 °C (Table 3) (Suvorova, 1974; Ohmoto and Rye, 1979). Except the highest one, the other calculated temperatures agree with the results obtained from fluid inclusion microthermometry. The examined fluid inclusions are primary in origin found in quartz of the veinlets. Six major fluid inclusion types are identified based on their shape and phase characteristics at room temperature including: monophase vapor (V type); two-phase vapor-rich (V-L); two-phase liquid-rich (L-V); simple brine (L-V-Halite); opaque-bearing brine (L-V-S), and multiphase brine (L-V- multiple opaque and transparent daughter phases). The homogenization temperature and salinity for V-L type is from 390 to 545 °C and from 1.57 to 5.07 wt% NaCl, respectively; for L-V type is from 269 to 345 °C and from 5.2 to 14.59 wt% NaCl, respectively; for L-V-H type is from 252 to 360 °C and from 29.24 to 52.91 wt% NaCl, respectively; for L-V-S type is from 345 to 525 and from 6.45 to 11.7 wt% NaCl, respectively and for the multiphase brine is between 53.64 and 71.35 wt% NaCl.

The calculated higher temperature (881°C) using pyrite-chalcopyrite pair (Ohmoto and Rye, 1979), probably reflects isotope disequilibrium. It could also be the artifact of anhydrite removal. Anhydrite is typically part of the original ore assemblage in these systems. However, it tends to be removed from the shallower parts of column or older pre-main stages relatively fast.

Additional data using pyrite-chalcopyrite (Ohmoto and Rye, 1979) and molybdenite-chalcopyrite and molybdenite-pyrite pairs (Suvorova, 1974) indicate temperatures of 329, 535, and 402 °C, respectively. These temperatures are compatible with those obtained from fluid inclusion microthermometry and show isotope equilibrium and analogous alteration type due to fluid evolution.

5. Concluding remarks

The Chah-Firouzeh PCD is the oldest member of PCDs in the Meiduk cluster, emplaced in the early-middle Miocene. Our zircon U–Pb dating results shows that the magma emplacement occurred between 16.91 ± 0.37 and 16.54 ± 0.23 Ma. This age range along with other dating studies conducted in the Meiduk cluster provides evidence for continuous post-collisional magmatic activity during the Miocene resulting to form several porphyry copper deposits and prospects in this region.

The molybdenite Re–Os dating on two samples show 16.60 ± 0.06 Ma and 15.99 ± 0.06 Ma for the mineralization. The results suggest that the duration of mineralization was at least 0.6 m.y. Comparison of these data with other Cu porphyry deposits and prospects of Meiduk cluster emphasizes that mineralization in this area is a relatively fast event. The plutonism timespan at the district scale is at least ~9.6 m.y., whereas Cu porphyry deposits formed in a few hundred thousand years pulses at the deposit scale. Rapid cooling plays an important role in providing ore fluids and development of hydrothermal alteration and mineralization.

Comparing the zircon U–Pb and molybdenite Re–Os ages reveals that mineralization occurred shortly after the intrusion of the Chah-Firouzeh porphyry and contemporaneously with the main stage of magma crystallization and continued during magma cooling and meteoric fluid influx.

The $\delta^{34}S$ values in the Chah-Firouzeh have a uniform and relatively narrow range (from −1.4 to +2.5‰) and demonstrate that the sulfur in the main stage of Chah-Firouzeh mineralization has a clearly mantle-dominated magmatic source.

Acknowledgments

This paper is a part of the first author's Ph.D. thesis at Tarbiat Modares University, Tehran, Iran. The authors would like to thank the Exploration Department of National Iranian Copper Industries Company (NICICo) for funding and providing access to exploration data and borehole cores. HM would like to thank CSIR-National Geophysical Research Institute, Hyderabad, India for providing U-Pb data from Shahre-Babak region. Here we just referred to the Chah-Firouzeh results. TVK and EVSSKB thank Dr. Y.J. Bhaskar Rao, the then-Director, CSIR-NGRI for giving permission for taking up this collaborative research work and they also thank the Director, CSIR-NGRI for permission to publish this article and use resources from the Projects INDEX WP-2.1 and MLP-6513-28-EVB. HM gives special thanks to the AIRIE Program for providing the Re-Os data. We thank Mohammad Maanijou and an anonymous reviewer for their constructive reviews on an earlier draft of the manuscript. Franco Pirajno and David Lentz are also thanked for careful editorial handling of the manuscript.

References

Agard, P., Omrani, J., Jolivet, L., Mouthereau, F., 2005. Convergence history across Zagros (Iran): constraints from collisional and earlier deformation. Int. J. Earth Sci. 94, 401–419. http://dx.doi.org/10.1007/s00531-005-0481-4.

Aghazadeh, M., Hou, Z., Badrzadeh, Z., Zhou, L., 2015. Temporal–spatial distribution and tectonic setting of porphyry copper deposits in Iran: Constraints from

zircon U-Pb and molybdenite Re–Os geochronology. Ore Geol. Rev. 70, 385–406. http://dx.doi.org/10.1016/j.oregeorev.2015.03.003.
Ahmad T., Posht Kuhi M., 1993. Geochemistry and petrogenesis of Urumiah-Dokhtar volcanic belt around Nain and Rafsanjan area; a preliminary study: treatise on the geology of Iran. Iranian Ministry of Mines and Metals. 90.
Alimohammadi, M., Alirezaei, S., Kontak, D.J., 2015. Application of ASTER data for exploration of porphyry copper deposits: a case study of Daraloo-Sarmeshk area, southern part of the Kerman copper belt, Iran. Ore Geol. Rev. 70, 290–304. http://dx.doi.org/10.1016/j.oregeorev.2015.04.010.
Alirezaei S., Hassanpour S., 2011. An overview of porphyry copper deposits in Iran. The 1st World Copper Congress. Tehran, Iran. pp. 17–32.
Alirezaei, S., Mohammadzadeh, Z., 2009. Hydrothermal Alteration-Mineralization at Chahfiroozeh Porphyry Copper Deposit, Kerman Province, Southern Iran. Joint Assembly. Geological Association of Canada, Canada.
Allègre, C.J., 2008. Isotope Geology. Cambridge University Press, New York. 1–534.
Allen, M.B., Jackson, J., Walker, R., 2004. Late Cenozoic reorganization of the Arabia-Eurasia collision and the comparison of short-term and long-term deformation rates. Tectonics 23, TC2008.
Asadi, S., Moore, F., Zarasvandi, A., 2014. Discriminating productive and barren porphyry copper deposits in the southeastern part of the central Iranian volcano-plutonic belt, Kerman region, Iran: A review. Earth-Sci. Rev. 138, 25–46. http://dx.doi.org/10.1016/j.earscirev.2014.08.001.
Atapour, H., Aftabi, A., 2007. The geochemistry of gossans associated with Sarcheshmeh porphyry copper deposit, Rafsanjan, Kerman, Iran: Implications for exploration and the environment. J. Geochem. Explor. 93, 47–65. http://dx.doi.org/10.1016/j.gexplo.2006.07.007.
Berberian, F., Muir, I.D., Pankhurst, R.J., Berberian, M., 1982. Late Cretaceous and early Miocene Andean-type plutonic activity in northern Makran and Central Iran. J. Geol. Soc. 139, 605–614.
Berberian, M., King, G.C.P., 1981. Towards a paleogeography and tectonic evolution of Iran. Can. J. Earth Sci. 18, 210–265. http://dx.doi.org/10.1139/e81-019.
Black, L.P., Kamo, S.L., Allen, C.M., Aleinikoff, J.N., Davis, D.W., Korsch, R.J., Foudoulis, C., 2003. TEMORA 1: A new zircon standard for Phanerozoic U-Pb geochronology. Chem. Geol. 200, 155–170. http://dx.doi.org/10.1016/S0009-2541(03)00165-7.
Cathles, L.M., Erendi, A.H.J., Barrie, T., 1997. How long can a hydrothermal system be sustained by a single intrusive event? Econ. Geol. 92, 766–771.
Corfu, F., Hanchar, J.M., Hoskin, P.W.O., Kinny, P., 2003. Atlas of zircon textures. Rev. Mineral. Geochem. 53, 469–500.
Dargahi, S., Arvin, M., Pan, Y., Babaei, A., 2010. Petrogenesis of post-collisional A-type granitoids from the Urumieh-Dokhtar magmatic assemblage, Southwestern Kerman, Iran: Constraints on the Arabian-Eurasian continental collision. Lithos 115, 190–204. http://dx.doi.org/10.1016/j.lithos.2009.12.002.
Del Rio-Salas, R., Ochoa-Landín, L., Valencia-Moreno, M., Calmus, T., Meza-Figueroa, D., Salgado-Souto, S., Kirk, J., Ruiz, J., Mendívil-Quijada, H., 2015. New U-Pb and Re–Os geochronology of Laramide porphyry copper mineralization along the Cananea lineament, northeastern Sonora, Mexico: Contribution to the understanding of the Cananea copper district. Ore Geol. Rev. 81, 1125–1136. http://dx.doi.org/10.1016/j.oregeorev.2015.11.029.
Dercourt, J., Zonenshain, L.P., Ricou, L.E., Kazmin, V.G., Le Pichon, X., Knipper, A.L., Grandjacquet, C., Sbortshikov, I.M., Geyssant, J., Lepvrier, C., Pechersky, D.H., Boulin, J., Sibuet, J.C., Savostin, L.A., Sorokhtin, O., Westphal, M., Bazhenov, M.L., Lauer, J.P., Biju-Duval, B., 1986. Evolution of the Tethys Geological evolution of the Tethys belt from the Atlantic to the Pamirs since the LIAS. Tectonophysics 123, 241–315. http://dx.doi.org/10.1016/0040-1951(86)90199-X.
Dimitrijevic, M.D., 1973. Geology of Kerman region. Geological Survey of Iran 334, 52.
Einali, M., Alirezaei, S., Zaccarini, F., 2014. Chemistry of magmatic and alteration minerals in the Chahfiruzeh porphyry copper deposit, south Iran: implications for the evolution of the magmas and physicochemical conditions of the ore fluids. Turkish J. Earth Sci. 23, 147–165.
Förster, H., 1978. Mesozoic-Cenozoic metallogenesis in Iran. J. Geol. Soc. 135, 443.
Gustafson, L.B., Hunt, J.P., 1975. The porphyry copper deposit at El Salvador, Chile. Econ. Geol. 70, 857–912. http://dx.doi.org/10.2113/gsecongeo.70.5.857.
Hassanzadeh, J., 1993. Metallogenic and tectono-magmatic events in the SE sector of the Cenozoic active continental margin of Iran (Shahr e Babak area, Kerman province) (Ph.D. thesis). University of California, Los Angeles, USA.
Honarmand, M., Ranjbar, H., Shahabpour, J., 2011. Application of spectral analysis in mapping hydrothermal alteration of the northwestern part of the kerman cenozoic magmatic arc, Iran. J. Sci. I R Iran 22, 17.
Jackson, S.E., Pearson, N.J., Griffin, W.L., Belousova, E.A., 2004. The application of laser ablation-inductively coupled plasma-mass spectrometry to in-situ U/Pb zircon geochronology. Chem. Geol. 211, 47–69.
John D.A., Ayuso R.A., Barton M.D., Blakely R.J., Bodnar R.J., Dilles J.H., Gray, Floyd, Graybeal F.T., Mars J.C., McPhee D.K., Seal R.R., Taylor R.D., Vikre P.G., 2010. Porphyry copper deposit model, 169.
Ludwig, K.R., 2003. Mathematical-statistical treatment of data and errors for 230Th/U geochronology. Rev. Mineral. Geochem. 52, 631–656.
Markey, R., Hannah, J.L., Morgan, J.W., Stein, H.J., 2003. A double spike for osmium analysis of highly radiogenic samples. Chem. Geol. 200, 395–406. http://dx.doi.org/10.1016/S0009-2541(03)00197-9.
Marsh, T.M., Einaudi, M.T., McWilliams, M., 1997. $^{40}Ar/^{39}Ar$ geochronology of Cu-Au and Au-Ag mineralization in the Potrerillos District, Chile. Econ. Geol. 92, 784–806.
McInnes B.I.A., Evans N.J., Belousova E., Griffin W.T., Andrew R.L., 2003. Timing of Mineralization and Exhumation Processes at the Sar Cheshmeh and Meiduk Porphyry Cu Deposits, Kerman Belt, Iran. 7th Biennial SGA Meeting, Athens, Millpress Rotterdam. pp. 1197–1200.
McInnes, B.I.A., Evans, N.J., Fu, F.Q., Garwin, S., 2005. Application of thermochronology to hydrothermal ore deposits. Rev. Mineral. Geochem. 58, 467–498.
Mirnejad, H., Mathur, R., Hassanzadeh, J., Shafie, B., Nourali, S., 2013. Linking Cu mineralization to host porphyry emplacement: Re-Os ages of molybdenites versus U-Pb ages of zircons and sulfur isotope compositions of pyrite and chalcopyrite from the Iju and Sarkuh porphyry deposits in southeast Iran. Econ. Geol. 108, 861–870. http://dx.doi.org/10.2113/econgeo.108.4.861.
Mohajjel, M., Fergusson, C.L., Sahandi, M.R., 2003. Cretaceous-Tertiary convergence and continental collision, Sanandaj-Sirjan Zone, western Iran. J. Asian Earth Sci. 21, 397–412. http://dx.doi.org/10.1016/S1367-9120(02)00035-4.
Mohammadzadeh, Z., 2009. Geology, alteration and copper mineralization in Chahfirouzeh area, Shahr-e-Babak, Kerman province (M.Sc thesis). Shahid Beheshti University, Iran (in Persian).
NICICo 2009. Final Report of Exploration in the Chahfiruzeh Deposit. National Iranian Copper Industries Co. in Persian. 185.
Ohmoto, H., Rye, R.O., 1979. Isotope of sulfur and carbon. In: Barnes, H.L. (Ed.), Geochemistry of Hydrothermal Deposits. second ed. Wiley, New York, pp. 509–567.
Pankhurst, M.J., Schaefer, B.F., Turner, S.P., Argles, T., Wade, C.E., 2013. The source of A-type magmas in two contrasting settings: U-Pb, Lu–Hf and Re–Os isotopic constraints. Chem. Geol. 351, 175–194. http://dx.doi.org/10.1016/j.chemgeo.2013.05.010.
Parsapoor, A., Dilles, J.H., Khalili, M., Mackizadeh, M.A., Maghami, M., 2014. Stable isotope record of hydrothermal sulfate, sulfide and silicate minerals in the Darreh-Zar porphyry copper deposit in Kerman, southeastern Iran: Implications for petrogenesis and exploration. J. Geochem. Explor. 143, 103–115. http://dx.doi.org/10.1016/j.gexplo.2014.03.025.
Richards, J.P., 2009. Postsubduction porphyry Cu-Au and epithermal Au deposits: products of remelting of subduction-modified lithosphere. Geology 37, 247.
Richards, J.P., Spell, T., Rameh, E., Razique, A., Fletcher, T., 2012. High Sr/Y magmas reflect arc maturity, high magmatic water content, and porphyry Cu ± Mo ± Au potential: examples from the Tethyan arcs of central and Eastern Iran and Western Pakistan. Econ. Geol. 107, 295–332.
Selby, D., Creaser, R.A., Stein, H.J., Markey, R.J., Hannah, J.L., 2007. Assessment of the 187Re decay constant by cross calibration of Re–Os molybdenite and U-Pb zircon chronometers in magmatic ore systems. Geochim. Cosmochim. Acta 71, 1999–2013. http://dx.doi.org/10.1016/j.gca.2007.01.008.
Shafiei, B., 2008. Transition from Paleogene normal calc-alkaline to Neogene adakitic-like plutonism and Cu-metallogeny in the Kerman porphyry copper belt: response to Neogene crustal thickening. J. Sci. I R Iran 19, 67–84.
Shafiei, B., 2010. Lead isotope signatures of the igneous rocks and porphyry copper deposits from the Kerman Cenozoic magmatic arc (SE Iran), and their magmatic-metallogenetic implications. Ore Geol. Rev. 38, 27–36. http://dx.doi.org/10.1016/j.oregeorev.2010.05.004.
Shafiei, B., Haschke, M., Shahabpour, J., 2009. Recycling of orogenic arc crust triggers porphyry Cu mineralization in Kerman Cenozoic arc rocks, southeastern Iran. Miner. Deposita 44, 265–283. http://dx.doi.org/10.1007/s00126-008-0216-0.
Shahabpour, J., Kramers, J.D., 1987. Lead isotope data from the Sar-Cheshmeh porphyry copper deposit, Iran. Miner Deposita 22, 278–281. http://dx.doi.org/10.1007/BF00204520.
Sillitoe, R.H., 2010. Porphyry copper systems. Econ. Geol. 105, 3–41.
Stein, H.J., 2014. Dating and tracing the history of ore formation. In: Holland, H.D., Turekian, K.K. (Eds.), Treatise on Geochemistry. second ed. Elsevier, Oxford, pp. 87–118.
Stein, H.J., Markey, R.J., Morgan, J.W., Hannah, J.L., Scherstén, A., 2001. The remarkable Re–Os chronometer in molybdenite: how and why it works. Terra Nova 13, 479–486. http://dx.doi.org/10.1046/j.1365-3121.2001.00395.x.
Suvorova V.A., 1974. Temperature dependance of the distribution coefficient of sulfur isotopes between equilibrium sulfides. National symposium on stable isotope geochemistry. Moscow p. 128 (in Russian).
Taghipoor, N., 2007. The Application of Fluid Inclusions and Isotope Geochemistry as Guides for Exploration, Alteration and Mineralization at the Miduk Porphyry Copper Deposit, Shahr-Babak, Kerman (Ph.D. thesis). Shaheed Bahonar University of Kerman (in Persian).
Taghipour, N., Aftabi, A., Mathur, R., 2008. Geology and Re-Os geochronology of mineralization of the Miduk porphyry copper deposit, Iran. Resour. Geol. 58, 143–160. http://dx.doi.org/10.1111/j.1751-3928.2008.00054.x.
Torrealday, H.I., Hitzman, M.W., Stein, H.J., Markley, R.J., Armstrong, R., Broughton, D., 2000. Re-Os and U-Pb dating of the vein-hosted mineralization at the Kansanshi copper deposit, northern Zambia. Econ. Geol. 95, 1165–1170. http://dx.doi.org/10.2113/gsecongeo.95.5.1165.
Valencia, V.A., Barra, F., Weber, B., Ruiz, J., Gehrels, G., Chesley, J., Lopez-Martinez, M., 2006. Re–Os and U-Pb geochronology of the El Arco porphyry copper deposit, Baja California Mexico: Implications for the Jurassic tectonic setting. J. South Am. Earth Sci. 22, 39–51. http://dx.doi.org/10.1016/j.jsames.2006.08.005.
Von Quadt, A., Erni, M., Martinek, K., Moll, M., Peytcheva, I., Heinrich, C.A., 2011. Zircon crystallization and the lifetimes of ore-forming magmatic-hydrothermal systems. Geology 39, 731–734.
Wang, Y., Zhao, C., Zhang, F., Liu, J., Wang, J., Peng, R., Liu, B., 2015. SIMS zircon U-Pb and molybdenite Re–Os geochronology, Hf isotope, and whole-rock geochemistry of the Wunugetushan porphyry Cu–Mo deposit and granitoid in NE China and their geological significance. Gondwana Res. 28, 1228–1245. http://dx.doi.org/10.1016/j.gr.2014.10.001.

Zimmerman, A., Stein, H.J., Hannah, J.L., Koželj, D., Bogdanov, K., Berza, T., 2008. Tectonic configuration of the Apuseni–Banat—Timok–Srednogorie belt, Balkans-South Carpathians, constrained by high precision Re–Os molybdenite ages. Miner. Deposita 43, 1–21. http://dx.doi.org/10.1007/s00126-007-0149-z.

Zimmerman, A., Stein, H.J., Morgan, J.W., Markey, R.J., Watanabe, Y., 2014. Re–Os geochronology of the El Salvador porphyry Cu–Mo deposit, Chile: Tracking analytical improvements in accuracy and precision over the past decade. Geochim. Cosmochim. Acta 131, 13–32. http://dx.doi.org/10.1016/j.gca.2014.01.016.